INL/EXT-14-31975

Comparison of Fission Product Release Predictions using PARFUME with Results from the AGR-1 Irradiation Experiment

Blaise P. Collin

September 2014

The INL is a
U.S. Department of Energy
National Laboratory
operated by
Battelle Energy Alliance

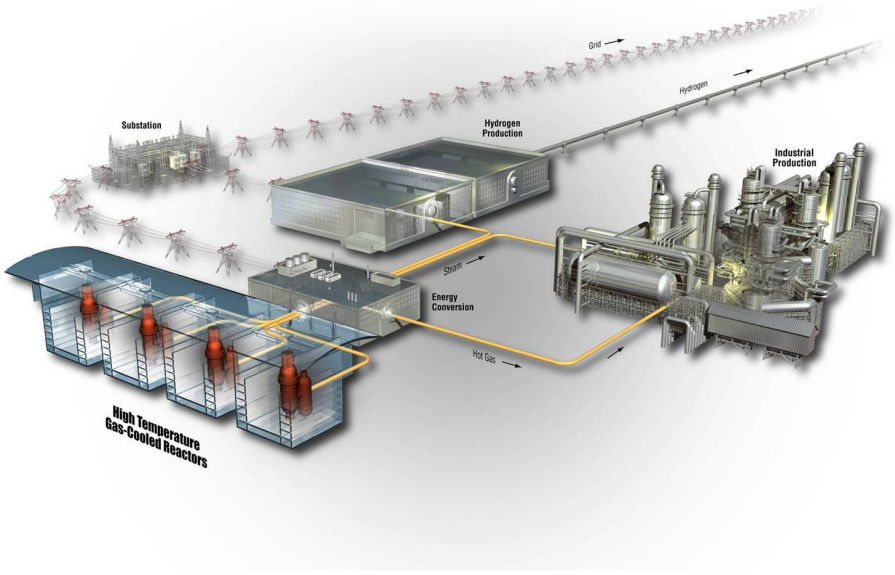

Idaho National Laboratory

INL/EXT-14-31975

Comparison of Fission Product Release Predictions using PARFUME with Results from the AGR-1 Irradiation Experiment

Blaise P. Collin

September 2014

Idaho National Laboratory
VHTR Program
Idaho Falls, Idaho 83415

http://www.inl.gov

Prepared for the
U.S. Department of Energy
Office of Nuclear Energy
Under DOE Idaho Operations Office
Contract DE-AC07-05ID14517

VHTR Program

Comparison of Fission Product Release Predictions using PARFUME with Results from the AGR-1 Irradiation Experiment

INL/EXT-14-31975

September 2014

Prepared by:

Blaise Collin — 9/9/2014

Blaise P. Collin — Date

Reviewed by:

Paul D — 9/9/14

Paul A. Demkowicz — Date
Technical Lead, Post Irradiation Examination

Approved by:

John T. Maki — 9-9-14

John T. Maki — Date
Technical Lead, Fuel Performance Modeling

David A. Petti — 9/9/14

David A. Petti, Director — Date
Very High Temperature Reactor Program

Kirk Bailey — 9-8-2014

Kirk Bailey — Date
Quality Assurance

REVISION LOG

Rev.	Date	Affected Pages	Revision Description
0	9/9/2014	All	Initial issue of the report

ABSTRACT

The PARFUME (PARticle FUel ModEl) code was used to predict fission product release from tristructural isotropic (TRISO) coated fuel particles and compacts during the first irradiation experiment (AGR-1) of the Advanced Gas Reactor Fuel Development and Qualification program.

The PARFUME model for the AGR-1 experiment used the fuel compact volume average temperature for each of the 620 days of irradiation to calculate the release of fission products silver, cesium, and strontium from a representative particle for a select number of AGR-1 compacts.

Post-irradiation examination (PIE) measurements provided data on release of fission products from fuel compacts and fuel particles, and retention of fission products in the compacts outside the silicon carbide (SiC) layer. PARFUME-predicted fractional release of these fission products was determined and compared to the PIE measurements.

Results show an overall overprediction of the fractional release of cesium by PARFUME. For particles with failed SiC layers, the overprediction is by a factor of about two, corresponding to an overestimation of the diffusivity in uranium oxycarbide (UCO) by a factor of about 100. For intact particles, whose release is much lower, the overprediction is by an average of about an order of magnitude, which could additionally be attributed to an overestimated diffusivity in SiC by about 30%.

The release of strontium from intact particles is also overestimated by PARFUME, which also points towards an overestimated diffusivity of strontium in either SiC or UCO, or possibly both. The measured strontium fractional release from intact particles varied considerably from compact to compact, making it difficult to assess the effective overestimation of the diffusivities. Furthermore, the release of strontium from particles with failed SiC is difficult to observe experimentally due to the release from intact particles, preventing any conclusions to be made on the accuracy or validity of the PARFUME predictions and the modeled diffusivity of strontium in UCO.

In the case of silver, the comparisons between PARFUME and PIE are better than for cesium and strontium. They show a trend of under-prediction at low burnup and overprediction at high burnup, but comparisons lie in the same order of magnitude. Modeling also confirmed the tendency of low burnup compacts to release more silver, and contributed to understanding that the broad range of the measured release was based in part on the large variation in temperatures in the compacts as a function of time during the irradiation as well as the wide range of spatially distributed temperatures across the compacts. Modeling limitations prevented the use of the detailed respective spatial distributions of temperature and burnup in the capsules. Instead, fission product release calculations had to rely on the use of volume-averaged temperatures and burnup.

CONTENTS

FIGURES

TABLES

ACRONYMS

AGR	Advanced Gas Reactor
AGR-1	first irradiation test of the AGR program
ASME	American Society of Mechanical Engineers
ATR	Advanced Test Reactor
BAF	Bacon Anisotropy Factor
CEGA	Combustion Engineering/General Atomics
DLBL	Deconsolidation-Leach-Burn-Leach
DOE	Department of Energy
EFPD	Effective Full Power Day
E_n	neutron energy
FIMA	Fissions per Initial heavy Metal Atom
HTGR	High Temperature Gas Reactor
IAEA	International Atomic Energy Agency
IMGA	Irradiated Microsphere Gamma Analysis
INL	Idaho National Laboratory
IPyC	Inner Pyrolytic Carbon
MFC	Materials and Fuels Complex
NQA	Nuclear Quality Assurance
PARFUME	PARticle Fuel ModEl
PIE	Post-Irradiation Examination
OPyC	Outer Pyrolytic Carbon
SiC	Silicon Carbide
TAVA	Time-Average Volume-Average
TMAP	Tritium Migration Analysis Program
TRISO	TRistructural ISOtropic
UCO	Uranium oxycarbide
UO_2	Uranium dioxide
VHTR	Very High Temperature Reactor

Comparison of Fission Product Release Predictions using PARFUME with Results from the AGR-1 Irradiation Experiment

1. INTRODUCTION

This report documents comparisons between post-irradiation examination measurements and model predictions of silver (Ag), cesium (Cs), and strontium (Sr) release from selected tristructural isotropic (TRISO) fuel particles and compacts during the first irradiation test of the Advanced Gas Reactor (AGR) program that occurred from December 2006 to November 2009 in the Advanced Test Reactor (ATR) at Idaho National Laboratory (INL).

The modeling was performed using the particle fuel model computer code PARFUME developed at INL. PARFUME is an advanced gas-cooled reactor fuel performance modeling and analysis code (Miller 2009). It has been developed as an integrated mechanistic code that evaluates the thermal, mechanical, and physico-chemical behavior of fuel particles during irradiation to determine the failure probability of a population of fuel particles given the particle-to-particle statistical variations in physical dimensions and material properties that arise from the fuel fabrication process, accounting for all viable mechanisms that can lead to particle failure. The code also determines the diffusion of fission products from the fuel through the particle coating layers, and through the fuel matrix to the coolant boundary. The subsequent release of fission products is calculated at the compact level (release of fission products from the compact) but it can also be assessed at the particle level by adjusting the diffusivity in the fuel matrix to very high values. Furthermore, the diffusivity of each layer can be individually set to a high value (typically 10^{-6} m^2/s) to simulate a failed layer with no capability of fission product retention.

During the AGR-1 irradiation campaign, the fuel kernel produced and released some fission products, which migrated through the successive layers of the TRISO-coated particle and potentially through the compact matrix. The release of these fission products was measured in PIE and modeled with PARFUME.

PARFUME calculates the release fraction as the ratio of the number of atoms released from the compact to the amount produced in the compact fuel kernels and through uranium contamination. The release fractions obtained during PIE were calculated by measuring the amount of fission products found outside of the particles and by normalizing that amount to a predicted end-of-irradiation total compact inventory obtained by as-run neutronics calculations of the AGR-1 experiment (Sterbentz 2013). In the case of silver, for which the release fraction is often relatively high, the release fraction can also be obtained by measuring the amount retained in the particles and/or compacts. The silver, cesium, and strontium release fractions determined by both PIE and PARFUME for selected compacts or TRISO-coated particles were then compared.

Section 2 gives a brief summary of the PIE measurements used for comparison to model predictions. Section 3 offers an overall overview of the AGR-1 experiment and its modeling with PARFUME. Comparisons between PIE and PARFUME on fission product release are made in Section 4 for silver and Section 5 for cesium and strontium. Conclusions are drawn in Section 6 and references are listed in Section 7.

The model predictions were completed using the code PARFUME developed at INL (Miller 2009). Calculations were performed with PARFUME Version 2.21.1.1 (as configured by the Revision Control System) compiled with Intel FORTRAN Compiler 11.1.073 on an SGI Altix ICE 8200 platform operating under SUSE Linux Enterprise Server 10. In addition, this study was conducted in accordance to quality standard NQA-1-2008; 1-a-2009 “Quality Assurance Requirements for Nuclear Facility Applications,” published by the American Society of Mechanical Engineers (ASME 2008).

2. AGR-1 IRRADIATION AND POST-IRRADIATION EXAMINATION

The Department of Energy (DOE) AGR Fuel Development and Qualification Program was established to qualify TRISO fuel for use in High Temperature Gas Reactors (HTGRs). The primary goal of the program is to provide a baseline fuel qualification data set in support of the licensing and operation of an HTGR (Simonds 2014).

Several fuel and material irradiation experiments are planned for the DOE AGR program. The goals of these experiments are to: provide irradiation performance data to support fuel process development, qualify fuel for normal operating conditions, support development and validation of fuel performance and fission product transport models and codes, and provide irradiated fuel and materials for post-irradiation examination and safety testing (Simonds 2014).

AGR-1 is the first of these irradiation tests. Irradiation began in the ATR in December 2006 and ended in November 2009. AGR-1 was intended to serve as a shakedown test of a multi-capsule design to be used in subsequent irradiations, and to test early variants of the fuel produced under the DOE AGR program (Maki 2009). A total of 72 compacts were irradiated in the AGR-1 experiment in six different capsules. The experiment completed 620 effective full power days (EFPD) in the reactor and achieved calculated peak burnup of 19.6% fissions per initial heavy metal atom (FIMA) and fast neutron fluence of 4.30×10^{25} n/m^2, $E_n > 0.18$ MeV (Collin 2014).

At completion of the irradiation, the AGR-1 test train was shipped to the Materials and Fuels Complex (MFC) at INL for PIE and high temperature safety testing. The objectives of the AGR-1 PIE and associated safety testing are to: assess the overall performance of the test train and components, provide data to verify the test train thermal analyses, verify the particle coating integrity, evaluate the fission product retention of the fuel during normal irradiation and during high temperature post-irradiation safety tests, and characterize the fuel compacts and individual particles to assess the condition of the matrix material, kernels, and coatings (Demkowicz 2010).

Comparison between PIE measurements and model predictions focused on silver, cesium, and strontium. Comparisons involving other fission products were not performed, either because of a lack of modeling input data for transport through TRISO particles and compacts for other species (e.g., europium), or because release was not observed in PIE (e.g., krypton). Specific irradiated compacts were selected for examination based on a detailed set of criteria, including the need to examine the different fuel types and to span a range of irradiation temperature and burnup.

Information on fission product release was obtained through a number of different measurements. The primary means of assessing the level of fission product release was through direct analysis of the released inventory, which included the inventory released from particles but retained in the compacts outside of the SiC layer and the inventory released from the compacts and measured on the irradiation capsule components. Silver represents a special case, in which the level of release can be sufficiently high (i.e., in excess of several percent) that the fraction retained can be estimated by measuring the remaining inventory in the fuel. In all cases, the measured inventory was first decay-corrected to the end of the AGR-1 irradiation and then compared with the predicted inventory from as-run neutronics calculations of the AGR-1 experiment to calculate corresponding release or retention fractions. The PIE data used for comparison with PARFUME predictions originate from four different measurement techniques (Demkowicz 2014):

- Gamma scanning of 56 irradiated AGR-1 compacts was used to determine their inventory of Ag-110m. The irradiation characteristics of these compacts are shown in Table 1: they include achieved burnup and fast fluence as well as Outer Pyrolytic Carbon (OPyC) time-average volume-average (TAVA) temperature of the compacts during the 620-day irradiation.

- Deconsolidation-leach-burn-leach (DLBL) was used on nine compacts to determine the amount of Cs-137 and Sr-90 that was retained within the compact outside of the SiC layer following irradiation. Table 2 lists the nine compacts that underwent DLBL.
- Irradiated microsphere gamma analysis (IMGA) was used to gamma count individual particles from these nine deconsolidated compacts in order to quantify their Ag-110m inventory.
- The inventory of fission products on the AGR-1 capsule components was measured to determine the level of release from the fuel compacts during irradiation.

IMGA and gamma scanning measure the inventory of fission products retained in the particles and compacts, respectively. DLBL measures the amount of fission products that diffused through the SiC layer and are retained in the OPyC layer or in the compact matrix. To assess the release from the particles, the amount of fission products released from the compact and found on capsule components must be taken into account. Fission product release from uranium contamination in the coating layers and in the matrix is included in the PIE measurements, but since the uranium contamination for AGR-1 was generally very low (the averages for each of the AGR-1 fuel types were lower than 4×10^{-7}) any release significantly above this level was attributed to release from the particles.

Measurements of the inventory remaining in the particles or compacts (e.g., IMGA for particles and gamma scanning for compacts) are not useful for determining the release of cesium and strontium, because the release fractions are very low (well under 1%). A more effective approach for these fission products is to directly analyze the relatively small inventory of fission products released from the fuel (e.g., DLBL data). On the other hand, because of the often large fractional release of silver from the fuel (which could range from 0 to 100% for particles and 0 to ~90% for compacts), measurement of the inventory remaining in the fuel can be an effective means of determining the release fraction, provided the total inventory generated during irradiation is known.

From PIE measurements, release fractions were calculated by normalizing the measured release to the total compact source predicted by as-run neutronics calculations (see Section 1). The measured release is the total release from the compact (gamma scanning), from all the particles in a compact (DLBL), or from a subset of particles (IMGA). In the case of DLBL measurements, the content of cesium and strontium found on capsule components was added to the content measured in the leached solution to reflect the total release from the particles.

Table 1. Compacts used for gamma scanning measurements.

Compact	Burnup (%FIMA)	Fast Fluence ($\times 10^{25}$ n/m^2, E_n > 0.18 MeV)	TAVA (°C)	Compact	Burnup (%FIMA)	Fast Fluence ($\times 10^{25}$ n/m^2, E_n > 0.18 MeV)	TAVA (°C)
6-2-3	14.17	2.90	1136	**3-4-2**	17.56	3.76	997
6-1-3	15.28	3.04	1112	**3-1-2**	17.58	3.72	993
6-2-2	12.05	2.55	1101	**3-4-1**	19.48	4.18	1025
6-1-2	12.79	2.68	1079	**3-3-1**	19.07	4.23	1051
6-4-1	13.35	2.43	1041	**3-1-1**	19.50	4.13	1023
6-3-1	13.53	2.67	1106	**2-4-3**	19.12	4.05	1015
5-3-3	17.01	3.65	1042	**2-3-3**	18.49	4.02	1032
5-2-3	17.42	3.77	1059	**2-2-3**	18.26	3.93	1022
5-1-3	18.19	3.82	1042	**2-4-2**	17.14	3.59	984
5-4-2	14.25	3.08	962	**2-3-2**	16.33	3.56	998
5-3-2	14.18	3.23	1002	**2-2-2**	15.97	3.48	987
5-2-2	14.64	3.33	1020	**2-1-2**	16.28	3.35	955
5-4-1	16.96	3.43	998	**2-4-1**	19.09	3.98	1013
5-3-1	16.93	3.60	1040	**2-3-1**	18.39	3.96	1029
5-2-1	17.37	3.71	1057	**2-2-1**	18.18	3.87	1020
5-1-1	18.22	3.76	1041	**2-1-1**	18.39	3.71	985
4-4-3	18.99	4.06	1059	**1-4-3**	17.36	3.39	1072
4-3-3	18.63	4.16	1094	**1-3-3**	16.30	3.27	1094
4-2-3	18.83	4.21	1101	**1-2-3**	15.60	3.10	1072
4-3-2	16.38	3.68	1057	**1-1-3**	15.32	2.86	1018
4-2-2	16.64	3.73	1065	**1-4-2**	14.93	3.01	1045
4-1-2	17.39	3.72	1042	**1-3-2**	13.82	2.90	1064
4-4-1	18.96	3.99	1057	**1-2-2**	13.35	2.74	1042
4-3-1	18.60	4.10	1092	**1-1-2**	13.22	2.52	989
4-2-1	18.81	4.15	1098	**1-4-1**	17.28	3.33	1071
3-4-3	19.56	4.24	1028	**1-3-1**	16.14	3.22	1092
3-2-3	19.12	4.28	1053	**1-2-1**	15.45	3.05	1071
3-1-3	19.53	4.20	1025	**1-1-1**	15.19	2.81	1017

Table 2. Compacts used for IMGA and DLBL measurements.

Compact	Burnup (%FIMA)	Fast Fluence ($\times 10^{25}$ n/m^2, $E_n > 0.18$ MeV)	TAVA (°C)
6-3-2	11.43	2.38	1070
6-1-1	15.25	3.00	1111
5-3-1	16.93	3.60	1040
5-2-3	17.42	3.77	1059
5-2-1	17.37	3.71	1057
4-4-2	16.74	3.59	1024
4-1-1	19.38	4.13	1072
3-2-1	19.07	4.21	1051
1-3-1	16.14	3.22	1092

3. PARFUME MODELING

3.1 AGR-1 Geometry and Fuel Characteristics

The AGR-1 test train was irradiated in the 38.1 mm (1.5 in.) diameter B-10 position of the ATR at INL. An ATR core cross section indicating this location is displayed in Figure 1. The test train contains six capsules arranged vertically as shown in Figure 2. Each AGR-1 capsule is 152.4 mm (6 in.) long and contains 12 fuel compacts arranged in three vertical stacks with each stack containing four compacts. Figure 3 illustrates a radial view of a capsule.

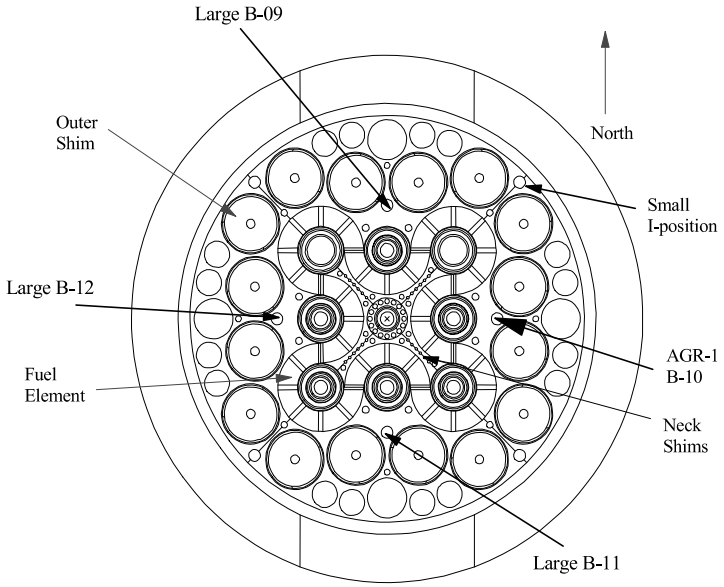

Figure 1. ATR core cross section displaying the B-10 position.

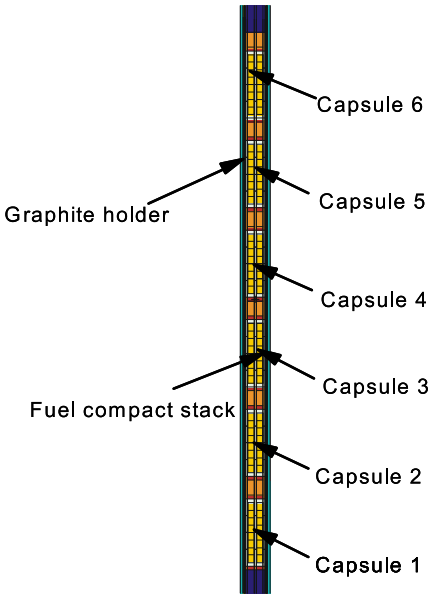

Figure 2. Axial schematic of the AGR-1 capsules.

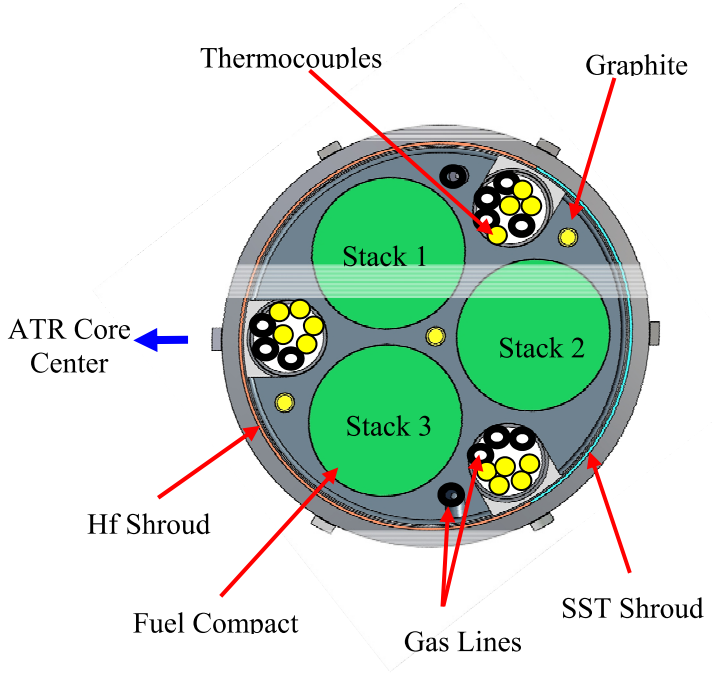

Figure 3. Radial schematic of an AGR-1 capsule.

AGR-1 compacts are right cylinders nominally 25.1 mm in length and 12.4 mm in diameter. Each compact contains ~4,100 fuel particles uniformly dispersed in a matrix composed of a thermosetting carbonaceous material. Each particle has a nominal diameter of ~800 µm and contains a kernel consisting of UCO fuel. The kernel is coated with a porous buffer layer to accommodate fission product accumulation, a SiC layer to retain the fission products, and inner and outer pyrocarbon (IPyC and OPyC) layers to protect the SiC as depicted in Figure 4. AGR-1 irradiation in ATR reached 620.2 EFPD (Collin 2014). Key aspects of the AGR-1 characteristics needed for PARFUME modeling are described below.

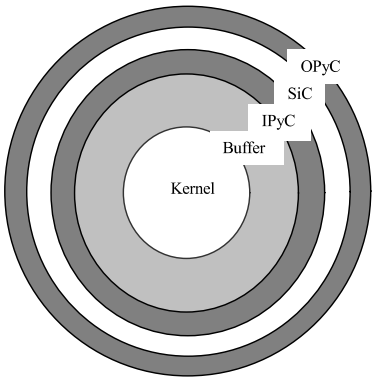

Figure 4. Schematic of a typical TRISO-coated fuel particle.

3.2 Boundary and Initial Conditions

PARFUME is designed to evaluate fuel performance based on user inputs for fast neutron fluence and burnup with a corresponding set of thermal conditions. The neutronics and thermal conditions for all the compacts used for comparison to PIE measurements are based on results obtained from as-run neutronics calculations and as-run thermal analysis (Sterbentz 2013, Hawkes 2012). The characteristics of the compacts are presented in Tables 1 and 2 (see Section 2). The calculations were computed prior to completion of PIE, and are based on an earlier version of the as-run neutronics calculations (Sterbentz 2011). The difference between the two sets of calculations is on burnup values, and does not exceed 1.2%. Therefore, there is no impact on the calculated results. All subsequent plots show the burnup values used in PIE analysis.

PARFUME assumes all particles in a compact experience similar irradiation and thermal histories over the course of irradiation. Practically, PARFUME models one particle using the average burnup and fast neutron fluence and the volume-averaged temperature of the whole compact. In this scheme, PARFUME statistically treats a collection of particles within a range of geometrical dimensions (see Table 3 in Section 3.3) but all the particles experience the same irradiation and thermal histories.

The 620 days of irradiation are modeled for each compact with end-of-irradiation values of burnup and fast neutron fluence displayed in Tables 1 and 2. Burnup and fast neutron fluence are assumed to evolve linearly during irradiation. The assumption is validated by the nearly linear increase of the compact burnup and fast neutron fluence values reached at the end of each AGR-1 cycle, as reported in the AGR-1 as-run report (Collin 2014).

The thermal history evolves on a daily basis. For each compact, the daily temperatures of all the calculation nodes are averaged, and PARFUME uses the resulting volume-averaged compact daily temperatures to set the thermal history of the modeled TRISO particle. The daily temperatures are set as boundary conditions at the outer edge of the OPyC. From the OPyC boundary temperature, PARFUME calculates the temperature profile between the OPyC and the kernel center, taking into account that the temperature profile is affected throughout irradiation by the width of the gap forming between the buffer and the IPyC layer.

Daily temperatures were used in modeling because the TAVA temperatures displayed in Tables 1 and 2 were determined to not be a suitable metric to correlate fission product release to temperature, as they do not adequately reflect the thermal state of the compacts throughout irradiation. The compacts experienced a range of daily volume-average temperatures that could span a few hundreds of degrees around their TAVA temperatures, resulting in a broad range of diffusivities, some of which far exceed the diffusivity values calculated at the TAVA temperatures. The diffusivities are modeled with an Arrhenius equation and exponentially decrease with inverse temperature (see Section 3.4). Consequently, diffusivity is highly sensitive to higher temperatures, and averaging higher and lower temperatures with similar weighs to compute fission product release with the resulting TAVA temperature leads to an under-estimation of the diffusivity, and hence to an under-estimation of the release.

As an illustration, Figure 5 shows the thermal histories of Compact 4-4-1 and Compact 4-3-2. Both compacts share the same TAVA temperature of 1057°C, but Compact 4-3-2 experienced higher temperatures over a larger period of time towards the end of irradiation. Compact 4-3-2 is therefore expected to yield a higher fractional release of fission products. In this example, the silver release fraction calculated with the TAVA temperature is 3%. Using their respective daily temperatures, release fractions of 18% for Compact 4-4-1 and 39% for Compact 4-3-2 are obtained, in accordance with the Arrhenius law abiding diffusivities. When compared to the PIE measurements of respectively 3% for Compact 4-4-1 and 42% for Compact 4-3-2, using the daily temperatures to calculate release fractions is a much better metric to account for the effect of temperature on fission product release.

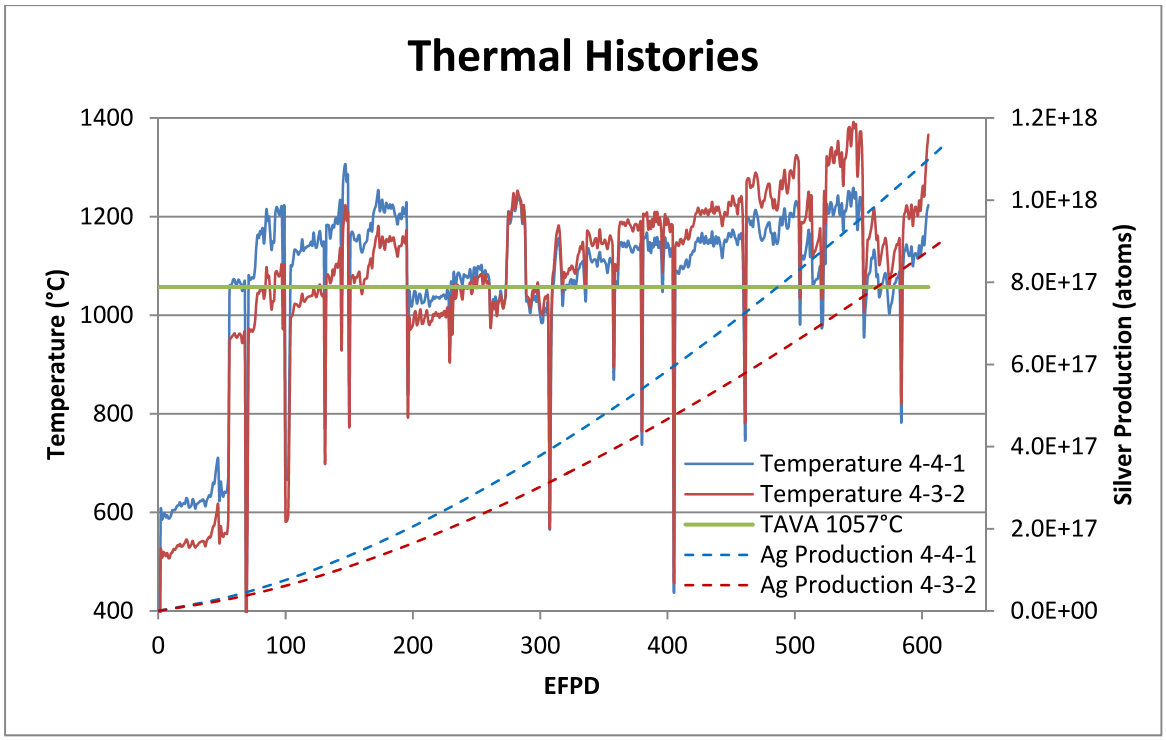

Figure 5. Evolution of daily temperatures and silver production throughout irradiation for Compact 4-4-1 and Compact 4-3-2.

3.3 Input Parameters

The input parameters needed to model the AGR-1 irradiation with PARFUME are listed in Table 3. They originate from:

- The AGR-1 Irradiation Experiment Test Plan (Maki 2009) for the fuel characteristics, particle geometry, compact characteristics, and material non-mechanical properties.
- A Combustion Engineering/General Atomics (CEGA) Corporation report (CEGA 1993) for the material mechanical properties.

Table 3. Parameters used in the PARFUME modeling of the AGR-1 irradiation.

Category	Parameter	Fuel type[a] Mean Value ± Standard Deviation		
		Baseline	Variant 1	Variant 3
Fuel characteristics	U235 enrichment (wt%)[b]	19.736		
	Oxygen/uranium (atomic ratio)[b]	1.3613		
	Carbon/uranium (atomic ratio)[b]	0.3253		
	Uranium contamination fraction[b]	3.64×10^{-7}	2.75×10^{-7}	1.26×10^{-7}
Particle geometry	Kernel diameter (μm)	349.7 ± 9.0		
	Buffer thickness (μm)	103.5 ± 8.2	102.5 ± 7.1	104.2 ± 7.8
	IPyC thickness (μm)	39.4 ± 2.3	40.5 ± 2.4	38.8 ± 2.1
	SiC thickness (μm)	35.3 ± 1.3	35.7 ± 1.2	35.9 ± 2.1
	OPyC thickness (μm)	41.0 ± 2.1	41.1 ± 2.4	39.3 ± 2.1
	Particle asphericity (SiC aspect ratio)	1.040		
Compact characteristics	Diameter (mm)	12.36	12.36	12.34
	Number of particles per compact	4154	4145	4132
	Compact matrix density (g/cm^3)	1.297	1.256	1.344
Material properties	IPyC Weibull modulus[b]	9.5		
	SiC Weibull modulus[b]	6.0		
	OPyC Weibull modulus[b]	9.5		
	IPyC / SiC bond strength (MPa)[c]	100.0		
	PyC Poisson's ratio in creep[b]	0.5		
	PyC creep coefficient amplifier	2.0		
	Kernel density (g/cm^3)[b]	10.924		
	Buffer density (g/cm^3)[b]	1.10		
	IPyC density (g/cm^3)[c]	1.904	1.853	1.904
	OPyC density (g/cm^3)[c]	1.907	1.898	1.911
	IPyC (post compact anneal) BAF[c]	1.022	1.014	1.029
	OPyC (post compact anneal) BAF[c]	1.019	1.013	1.021
Boundary conditions	Ambient pressure (MPa)	0.1		

a. Baseline fuel in Capsules 3 and 6, Variant 1 in Capsule 5, and Variant 3 in Capsules 1 and 4.
b. Standard deviation not considered in PARFUME.
c. Standard deviation not included in these AGR-1 calculations.

In addition, as-run neutronics calculations and as-run thermal analysis are used for the boundary conditions (see Section 3.2), and diffusion coefficients used for fission product transport are derived from the International Atomic Energy Agency (IAEA) Technical Document 978 (IAEA 1997) (see Section 3.4).

As indicated in Table 3, a baseline fuel type and two fuel variant types are tested. Baseline fuel is used in Capsules 3 and 6, Variant 1 fuel is used in Capsule 5, and Variant 3 fuel is used in Capsules 1 and 4. Statistical variations are considered relative to the fuel particle geometry only (kernel diameter, buffer, pyrolytic carbon (PyC), and SiC thicknesses). PARFUME also has the capability to address statistical variations in creep, bond strength, PyC densities, and PyC Bacon Anisotropy Factors (BAF). With the exception of creep and bond strength, the AGR-1 Irradiation Experiment Test Plan (Maki 2009) provides information regarding these variations. However, results from sensitivity calculations indicated these variations have little impact on the probability of AGR-1 fuel particle failure (Miller 2007). Because the effects are so small, statistical variations in PyC densities and BAF are not considered in these AGR-1 calculations.

The asphericity mentioned in Table 3 is considered at the SiC layer, as required by PARFUME inputs. Asphericity measurements reported in the AGR-1 Irradiation Experiment Test Plan correspond to asphericity at the OPyC layer. The asphericity of AGR-1 fuel particles at the SiC layer was not measured during the coating process, but post-coating optical inspection showed asphericity at that layer is limited. Asphericity at the SiC layer was measured at a mean value of 1.037 for AGR-2 UCO fuel (Collin 2011). Therefore, a value of 1.040 is a conservative upper limit. Furthermore, previous sensitivity studies concluded variations in asphericity at this level had a negligible impact on the probability of AGR-1 fuel particle failure (Miller 2007).

The material mechanical properties used in PARFUME are obtained from a report compiled by the CEGA Corporation (CEGA 1993). Table 3 displays parameters used in PARFUME user inputs. Material properties directly incorporated into the PARFUME code source are discussed by (Miller 2007 & 2009).

3.4 Fission Product Transport

Fission product transport in PARFUME is based on coding extracted from the Tritium Migration Analysis Program Version 4 (TMAP4) computer code. Originally developed to assist in the evaluation of tritium losses from fusion reactor systems, TMAP4 incorporates a one-dimensional diffusion capability that determines the thermal response of structures and solves equations for solute atom movement through surfaces and in bulk materials (Longhurst 1992).

The coding extracted from TMAP4 was modified for use within PARFUME to calculate fission product transport from the kernel through the successive coating layers of a TRISO-coated fuel particle, from individual TRISO-coated fuel particles to the surrounding matrix, and from the surrounding matrix to the outside of the fuel sphere or compact, which constitutes the release of the fission products.

Fission product transport in PARFUME is a three-step process that includes a fuel element thermal analysis, thermal and fission product transport analyses for fuel particles, and a fuel element fission product transport analysis ultimately leading to fission product release. Thermal analyses are performed to acknowledge the temperature dependence of diffusion. Diffusion is first calculated for individual fuel particles. Results from each particle then serve as time- and position-dependent fission product sources for the subsequent fuel element transport analysis.

Fission product transport was calculated for the three following fission products: silver (Ag), cesium (Cs), and strontium (Sr). Diffusion coefficients used in PARFUME for each of these species in the successive coating layers and matrix are derived from the IAEA (IAEA 1997) and displayed in Table 4. The corresponding diffusivities can be calculated using these diffusion coefficients in the following Arrhenius-type equation:

$$D = D_{0,1} e^{-\frac{Q_{0,1}}{RT}} + D_{0,2} e^{-\frac{Q_{0,2}}{RT}}$$

where

$D_{0,i}$ = pre-exponential factor (m^2/s)
$Q_{0,i}$ = activation energy (kJ/mol)
R = gas constant (8.3142×10^{-3} kJ/mol/K)
T = temperature (K)

Table 4. Diffusion coefficients used in PARFUME.

Species	$D_{0,i}$ (m^2/s) $Q_{0,i}$ (kJ/mol)	Kernel[a]	Buffer	IPyC / OPyC	SiC	Matrix graphite[b]
Ag	$D_{0,1}$ $Q_{0,1}$	6.7×10^{-9} 165	10^{-8} 0	5.3×10^{-9} 154	3.6×10^{-9} 215	1.6 258
	$D_{0,2}$ $Q_{0,2}$	-	-	-	-	-
Cs	$D_{0,1}$ $Q_{0,1}$	5.6×10^{-8} 209	10^{-8} 0	6.3×10^{-8} 222	5.5×10^{-14} 125	3.6×10^{-4} 189
	$D_{0,2}$ $Q_{0,2}$	5.2×10^{-4} 362	-	-	1.6×10^{-2} 514	-
Sr	$D_{0,1}$ $Q_{0,1}$	2.2×10^{-3} 488	10^{-8} -	2.3×10^{-6} 197	1.2×10^{-9} 205	10^{-2} 303
	$D_{0,2}$ $Q_{0,2}$	-	-	-	1.8×10^{6} 791	-

a. Kernel diffusivities are obtained from UO_2 data.
b. Diffusivity in the matrix was set to 10^{-6} m^2/s in the IMGA (Ag) and DLBL (Cs and Sr) modeling to allow access to the release at the particle level.

The diffusion coefficients in Table 4 have been derived from the evaluation of numerous irradiation and heating experiments. They are defined as “effective” diffusion coefficients, “effective” meaning that all possible transport mechanisms are summarized in a single transport process. The use of these effective diffusion coefficients is to be considered with care. These coefficients were determined for uranium dioxide (UO_2) fuel and associated particle coatings of older German fabrication, whose properties are different than these of the UCO fuel of the AGR-1 experiment. Furthermore, in many cases, they are partly based on data from post-irradiation heating tests, which do not take into account the irradiation effects and are conducted at higher temperatures than usual irradiation experiments. Consequently, IAEA diffusivities are not necessarily well adapted to model fission product transport of the AGR-1 irradiation experiment.

Figures 6 through 8 display the diffusivities of silver, cesium, and strontium as a function of temperature in the successive layers of a particle and compact. From these plots, the following conclusions can be drawn:

- Silver: SiC is the main retention barrier, but the kernel is also slightly retentive. Considering the dimensions of the TRISO particle, the diffusion time through the kernel is not negligible compared to the diffusion time through the SiC layer. However, at the AGR-1 temperatures these diffusion times are small compared to the irradiation length and silver is not predicted to be well retained over the course of irradiation.
- Cesium: as with silver, the SiC layer is the main retention barrier, but to a much larger extent than the kernel. However, the kernel is more retentive to cesium than it is to silver, which is an important factor in the case of particles with failed SiC layers. Because of its lower diffusivities, cesium is better retained than silver in both the kernel and the SiC layer.
- Strontium: unlike cesium and silver, strontium is primarily retained by the kernel itself. The combination of a larger thickness and a lower diffusivity compared to the SiC layer makes the kernel the main retention barrier. Therefore, strontium release is less affected by a failure of the SiC layer and, because of its low kernel diffusivity, strontium is well retained by the TRISO fuel at the AGR-1 temperatures.

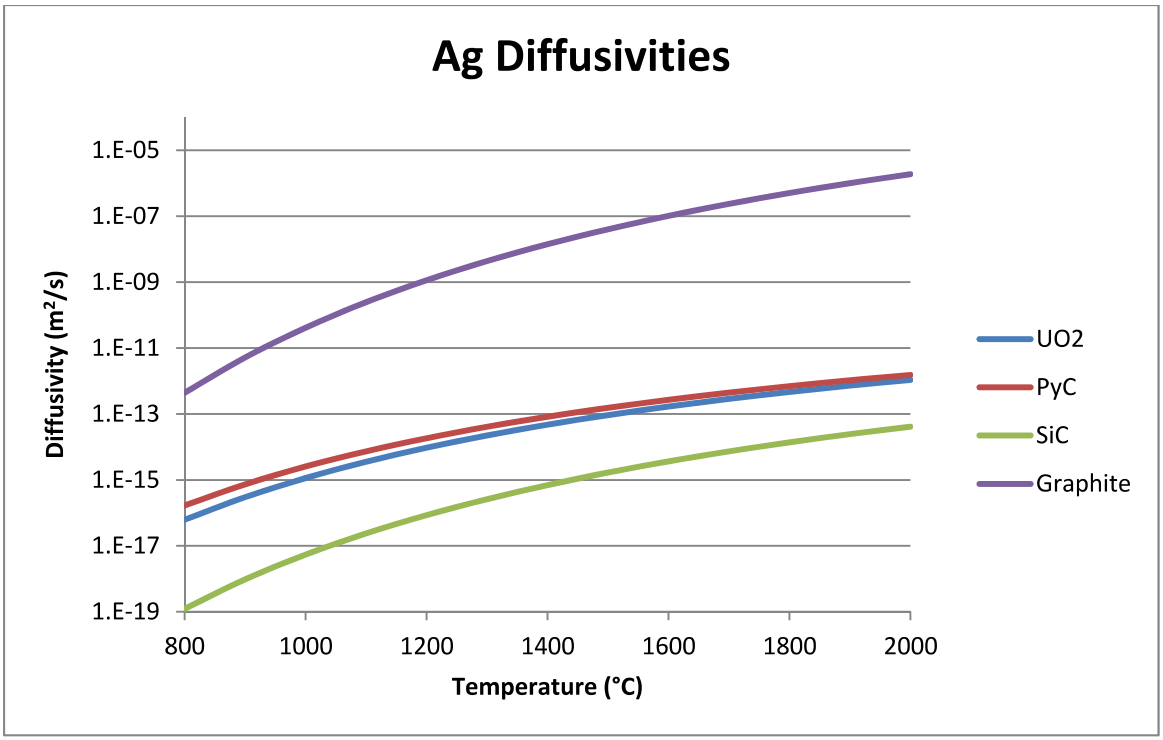

Figure 6. Silver diffusivities.

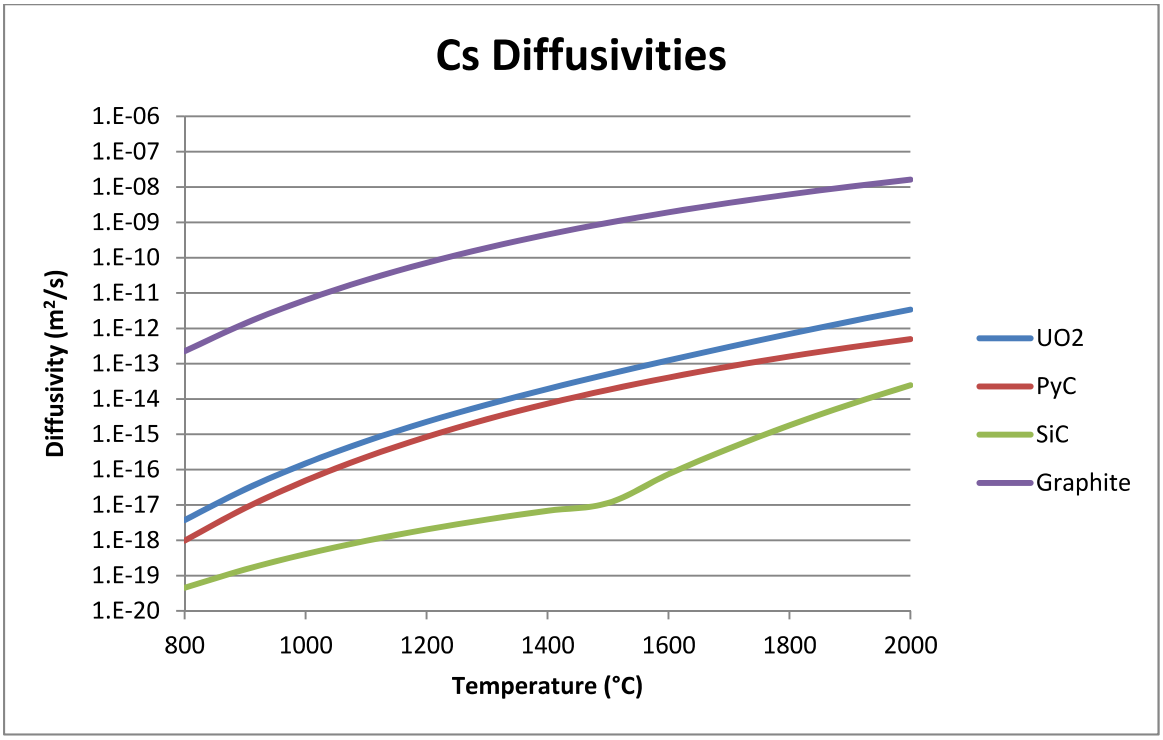

Figure 7. Cesium diffusivities.

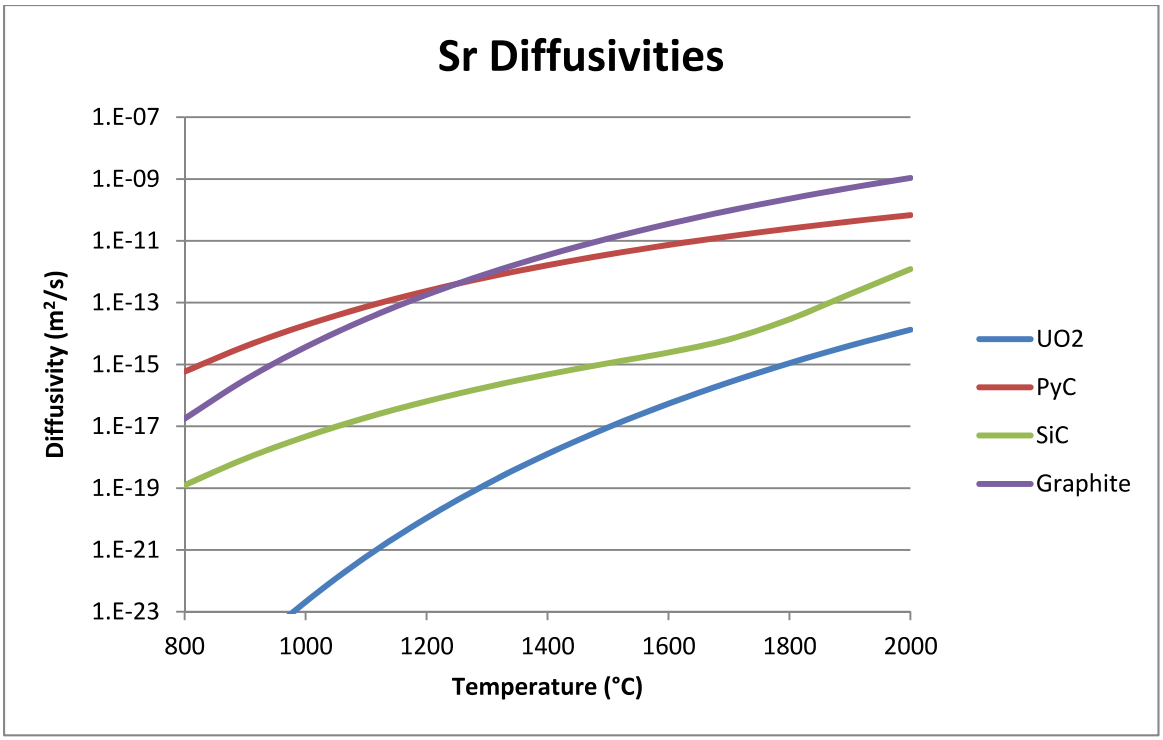

Figure 8. Strontium diffusivities.

The release of fission products is calculated at the compact level after the fission products were transported through the TRISO particle and the surrounding compact, and subsequently released to the capsule graphite holder. The capsule holder is not modeled in PARFUME and fission products are considered released once they reach the compact edge. The fractional release of fission products is then calculated by normalizing the calculated release from the compact to the calculated kernel source. Capsule components are analyzed during PIE to account for any release from the AGR-1 compacts (Demkowicz 2013).

To access the release at the particle level, i.e., the amount of fission products that are released from the TRISO particle into the compact matrix, PARFUME can be modified to force diffusion through the matrix. This is done by adjusting the diffusivity of the matrix graphite to a value of 10^{-6} m^2/s. With this adjustment, the release PARFUME calculates at the edge of the compact actually corresponds to the release from the TRISO particle.

In PARFUME, the calculation of fission product transport through a collection of particles is weighted by the probability of failure of these particles. The statistical variations in the modeling parameters of Table 3 (see Section 3.3) are used to determine any layer failure, at which point the diffusivity of that layer is set to 10^{-6} m^2/s, corresponding to a loss of retentive capability. This relies on the strong assumption that a failed layer does not retain diffusing species at all, even partially, and it is implemented as such for lack of a better understanding of the diffusing mechanisms in failed layers. The resulting release from the collection of particles includes release from intact particles as well as release from particles with failed coating layers as determined by the stress analysis. To more accurately reproduce the number of particles with non-retentive coating layers potentially observed in PIE, or lack thereof, it was decided to model intact particles and particles with failed layers separately. In PARFUME, this requires decoupling of the stress and fission product transport calculations. This is achieved by inhibiting the calculation of failures originating from multi-dimensional effects, which in this study are the main contributors to particle failure. The code can then be modified to separately model intact particles and particles with failed layers in the TRISO fuel, by setting the diffusivities of fission products

in these layers to the same value of 10^{-6} m^2/s. This results in separate release fractions from intact particles and from particles with failed layers, which can then be combined accordingly in each compact to compare to the measured release data. For cesium and strontium, the IPyC layer is not very retentive, and there is a negligible difference in release from a particle with failed SiC and intact IPyC and a particle with both layers failed. In this study, PARFUME models both intact particles and particles with both failed IPyC and SiC layers. Also, because the timing of potential failures during irradiation is not known, PARFUME assumes failed layers from the start of irradiation. Failure probability calculations on AGR-1 fuel showed that the SiC tangential stress was maximum after around 100 EFPD, indicating that potential failures would occur early during irradiation (Miller 2007). The assumption made in PARFUME therefore theoretically shifts the release of fission products through failed coating layers by about 100 days.

4. SILVER RELEASE

Gamma scanning of 56 compacts was used to measure the retained Ag-110m at the compact level. In addition, IMGA on particles from nine deconsolidated compacts was used to estimate the average retention in the particles from each compact.

4.1 Compact Gamma Scanning

Gamma scanning was performed on the 56 irradiated compacts listed in Table 1 (see Section 2) to determine their inventories of Ag-110m. The irradiation characteristics of the compacts cover a wide range of burnup, fast fluence, and TAVA temperature, as can be seen in the three-dimensional plot of Figure 9 and the two-dimensional projections in Appendix A.

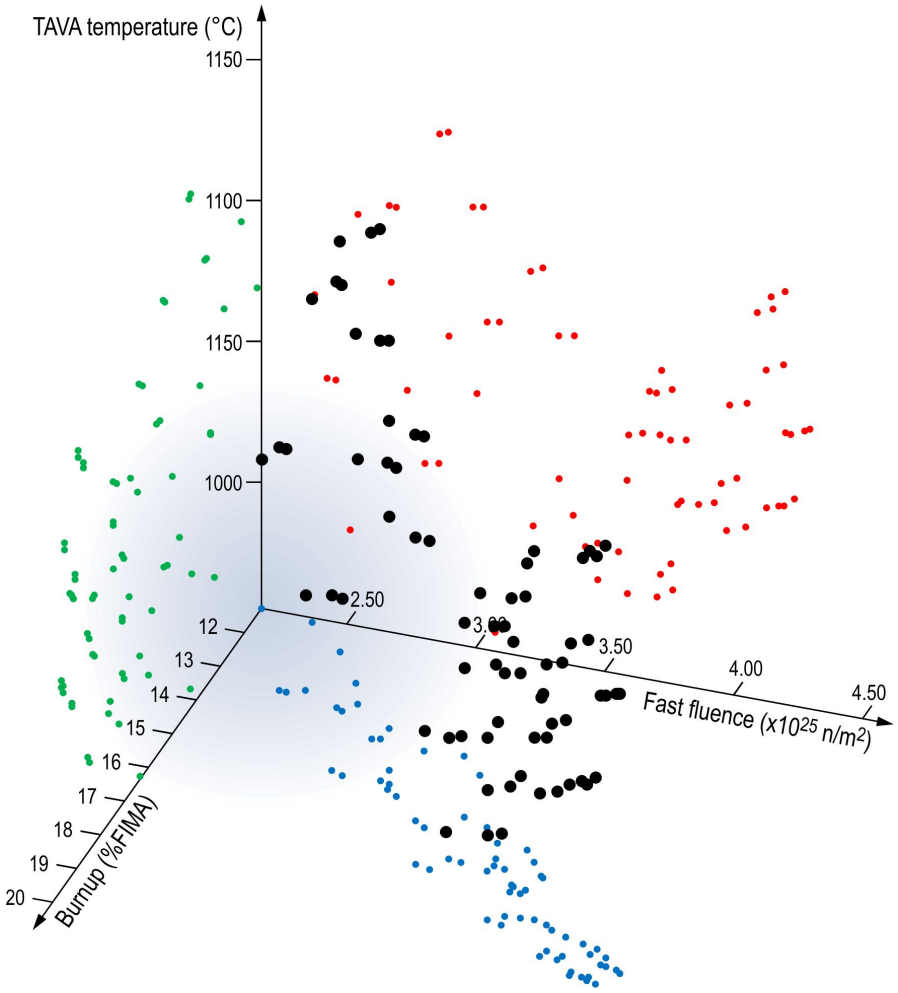

Figure 9. Distribution of the 56 gamma scanned AGR-1 compacts.

The silver release was assessed at the compact level (see Section 3.4), by compact gamma scanning to measure the inventory of silver retained in the compact. The retention fraction was obtained by dividing the retained inventory by the total inventory of silver produced during irradiation, as calculated by as-run neutronics. The release fraction is equal to 1 minus the retention fraction. PIE measurements (Harp 2013) and PARFUME predictions for the 56 selected compacts are displayed in Figure 10. Compacts in Figure 10 are numbered in the order presented in Table 1. Appendix B displays break-down plots for each capsule, from which the following observations can be made:

- PARFUME under-predicts the PIE data in Capsule 1 and Capsule 6
- PARFUME under-predicts the PIE data in Capsule 5 on average
- PARFUME overpredicts the PIE data in Capsule 2 and Capsule 3
- PARFUME mostly overpredicts the PIE data in Capsule 4.

Referring to Table 1 (see Section 2), it means that PARFUME underpredicts PIE data in the lower burnup capsules and overpredicts PIE data in the higher burnup capsules. Note that there is an apparent bias in the measured values, indicated by the silver release values that are negative in the plot. This results from the measured Ag-110m inventories being slightly higher than the predicted inventories for those compacts. This could be due to experimental uncertainty in the measured Ag-110m inventories, a bias in the predicted Ag-110m inventories (in this case, the indication is that the predicted values are low), or both.

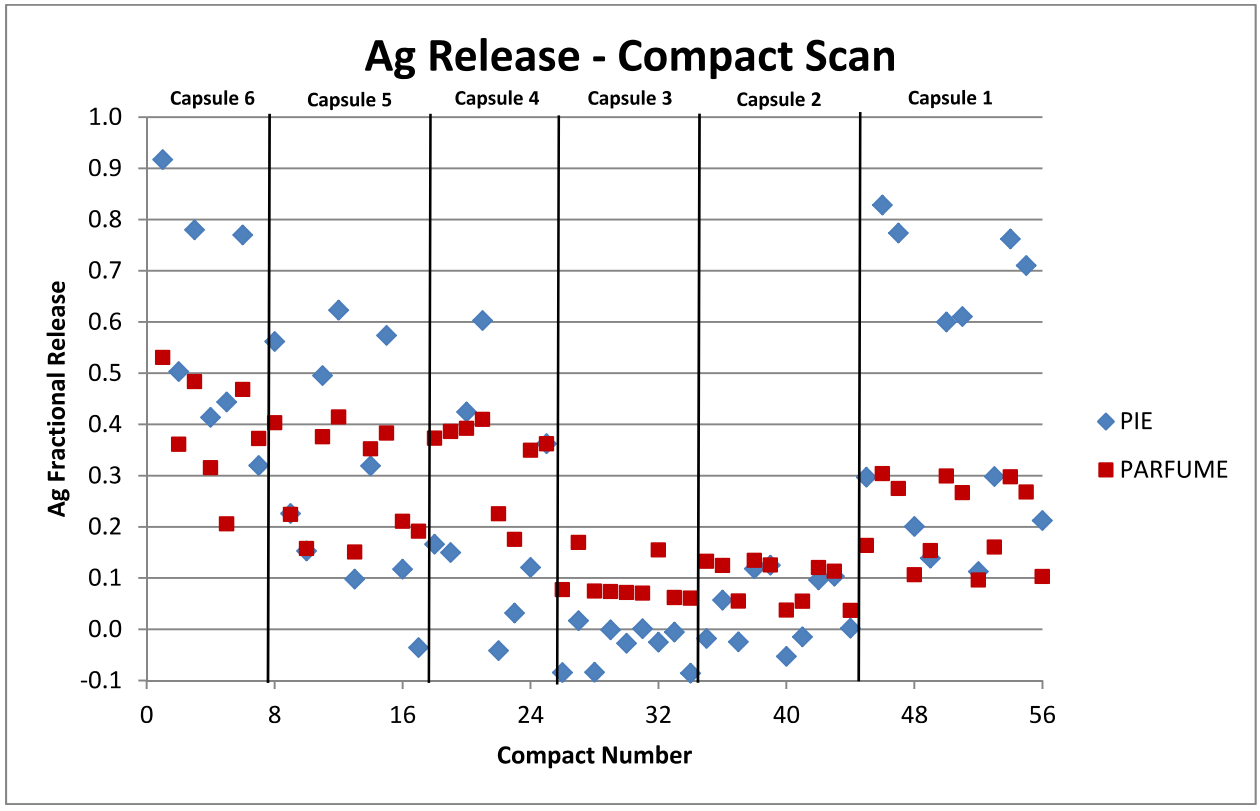

Figure 10. Silver release from compact gamma scanning (numbering follows order of Table 1).

4.2 Irradiated Microsphere Gamma Analysis

IMGA was performed on particles from the nine compacts listed in Table 2 (see Section 2). Typically 40 to 120 particles were selected per compact. The silver retention fraction was determined for each particle by calculating the ratio of the measured Ag-110m inventory to the predicted inventory. The average particle retention fraction for each compact was then calculated by averaging the individual particle values. The average silver release fraction (1 – "measured retention fraction") per particle was then compared to the values calculated by PARFUME.

PIE results (Demkowicz 2014) and PARFUME results are displayed in Figure 11. Similar to the compact gamma scanning comparisons, PARFUME overpredicts release for compacts taken from Capsule 3 and Capsule 4, and it under-predicts release for compacts from Capsule 1, Capsule 5 and Capsule 6.

PIE data for Compacts 1-3-1, 5-2-1, 5-2-3, 5-3-1, and 6-3-2 show a range that accounts for uncertainty in the average particle retention fraction due to several gamma-counted particles from each compact exhibiting Ag-110m inventory below the detection limit. Using the detection limit for the activity results in an upper bound for the total average retention while using zero results in a lower bound for the total average retention. These two limits set the range for the release fractions shown in Figure 11.

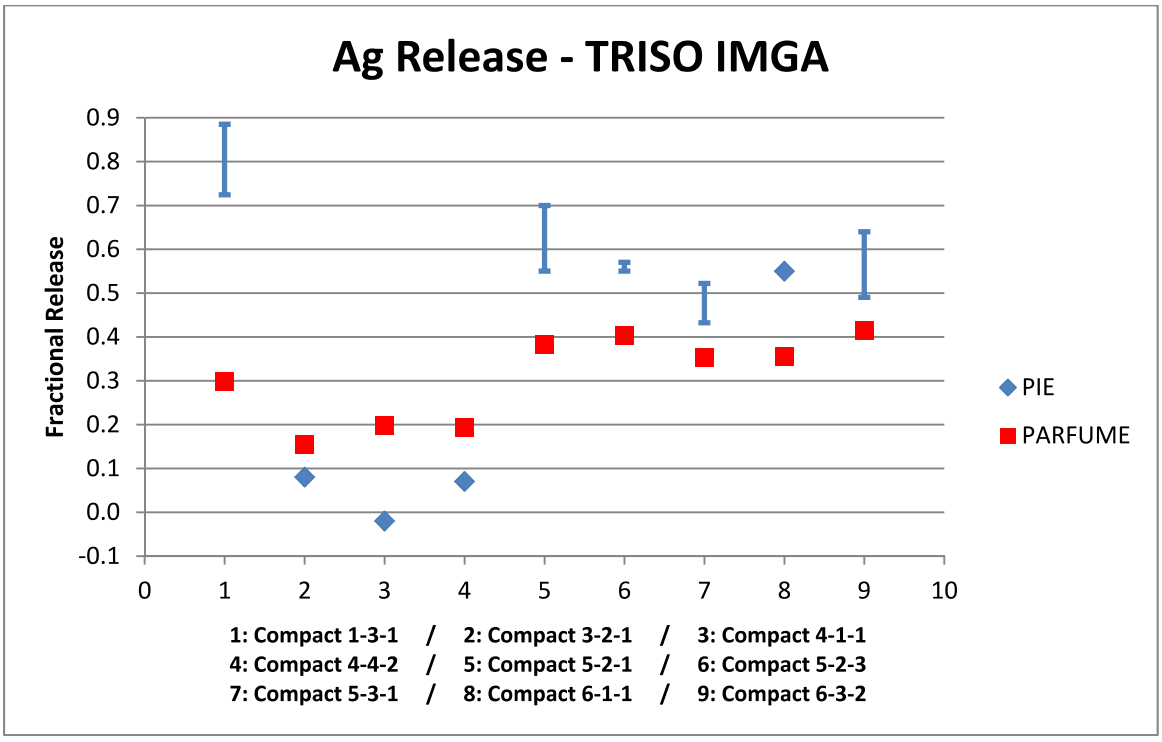

Figure 11. Silver release from IMGA. The bars for PIE data of Compacts 1-3-1, 5-2-1, 5-2-3, 5-3-1, and 6-3-2 show the range of measurements that arise from setting the activity below detection limit at zero or at the detection limit.

The PIE and PARFUME data displayed in Figure 11 are subject to uncertainties that arise from limited knowledge of physical properties such as the silver fission yield used to assess the silver inventory (PIE and PARFUME), or the diffusion coefficients (PARFUME). These uncertainties were not assessed in this study.

4.3 Silver Matrix Content

Sections 4.1 and 4.2 showed reasonable agreement between PIE and PARFUME for silver release from compacts or particles. In the case of PARFUME, the calculated release from particles or from their host compact is essentially identical because of the high diffusivity assumed for silver in the matrix material (see Table 4). Direct PIE measurements performed by DLBL on the compacts in Table 2 (see Section 2) showed that the amount of silver outside the SiC layer (referred to here as "matrix content", even though the experimental technique cannot distinguish between inventory in the OPyC or in the matrix) is generally limited to a small percent of the silver inventory or less, with the exception of Compact 6-1-1, whose silver matrix content reaches 12% (Demkowicz 2012). On the other hand, results from the AGR-1 safety testing experiments showed on a few occasions a high release of silver, up to 30%, in the first hours of the tests (Morris 2014). Based on the nature of this prompt release, it is believed it comes primarily from silver that was released from particles during the irradiation but retained within the compacts outside of the SiC layer, and subsequently rapidly released when the compacts were heated to 1600°C. To a first approximation then, these rapid silver releases are taken as a measure of silver outside of the SiC layer in the compacts, comparable to the DLBL measurements.

Table 5 shows the measured (DLBL) or estimated (safety testing) matrix content for the compacts for which such measurements are available. Note that the values for silver in the matrix of compacts based on safety test data are based on the assumption that the early release from these compacts represents the silver content in the matrix, but that this value was not measured directly. Table 5 also shows the fractional release measured by gamma scanning and calculated by PARFUME. Combining the measurements from gamma scanning and matrix content gives an assessment of the fractional release from the particles. In the table, some of the PIE release fractions were not directly available and were assessed from neighboring compacts (analysis of available PIE data from neighboring compacts indicates that the level of silver in the matrix of the two compacts was similar).

Table 5. Compact matrix content.

Compact	PIE Compact Release Fraction[a]	Matrix Content[b,c]	PIE Corrected Release Fraction	PARFUME Release Fraction
6-4-3	0.44 [a]	1.9×10^{-2} [b]	0.46	0.21
6-4-1	0.44	3.1×10^{-2} [b]	0.48	0.21
6-2-1	0.92 [a]	2.9×10^{-3} [b]	0.92	0.52
6-1-1	0.50 [a]	1.2×10^{-1} [c]	0.62	0.36
5-3-3	0.32	2.0×10^{-2} [b]	0.34	0.37
5-2-3	0.56	3.3×10^{-3} [c]	0.57	0.40
5-1-3	0.23	3.9×10^{-2} [b]	0.27	0.22
5-3-1	0.32	9.3×10^{-3} [c]	0.33	0.35
4-4-3	-0.04	1.6×10^{-1} [b]	0.13	0.19
4-3-3	0.17	3.4×10^{-1} [b]	0.50	0.37
4-3-2	0.42	6.2×10^{-2} [b]	0.49	0.39
4-1-2	-0.04	5.7×10^{-2} [b]	0.01	0.23
4-4-1	0.03	1.2×10^{-1} [b]	0.15	0.18
3-2-3	0.02	8.9×10^{-2} [b]	0.11	0.17
3-3-1	-0.03	5.0×10^{-2} [b]	0.02	0.15
3-2-1	0.02 [a]	6.7×10^{-3} [c]	0.02	0.16
1-3-1	0.76	3.6×10^{-3} [c]	0.77	0.30

a. Value from neighbor compact.
b. Matrix content from safety testing analysis.
c. Matrix content from DLBL data.

Using results from Table 5, Figure 12 shows how both initial and corrected PIE results compare to PARFUME results, for which compact release and particle release are essentially identical. In Figure 12, the data labeled “PIE” is based solely on the total compact inventory data (from gamma scanning) and is identical to that presented in Figure 10 for these specific compacts. The data labeled “Corrected PIE” has been determined as described in this paragraph (i.e., correcting the total compact inventory by the amount estimated to be present in the compact outside the SiC layer at the end of irradiation). PARFUME does not predict any silver retention outside the SiC layer, hence it only has one set of results. Compacts in Figure 12 are numbered in the order presented in Table 5. Figure 12 shows the previously observed trends of under/overpredictions are mostly not modified by the correction of the matrix content. In the case of under-prediction, the discrepancy between PIE and PARFUME is increased, while in the case of overprediction, the corrected PIE results are closer to the PARFUME results. The exception is Compact 4-3-3 (No. 10 in Figure 5) that goes from being overpredicted to being under-predicted.

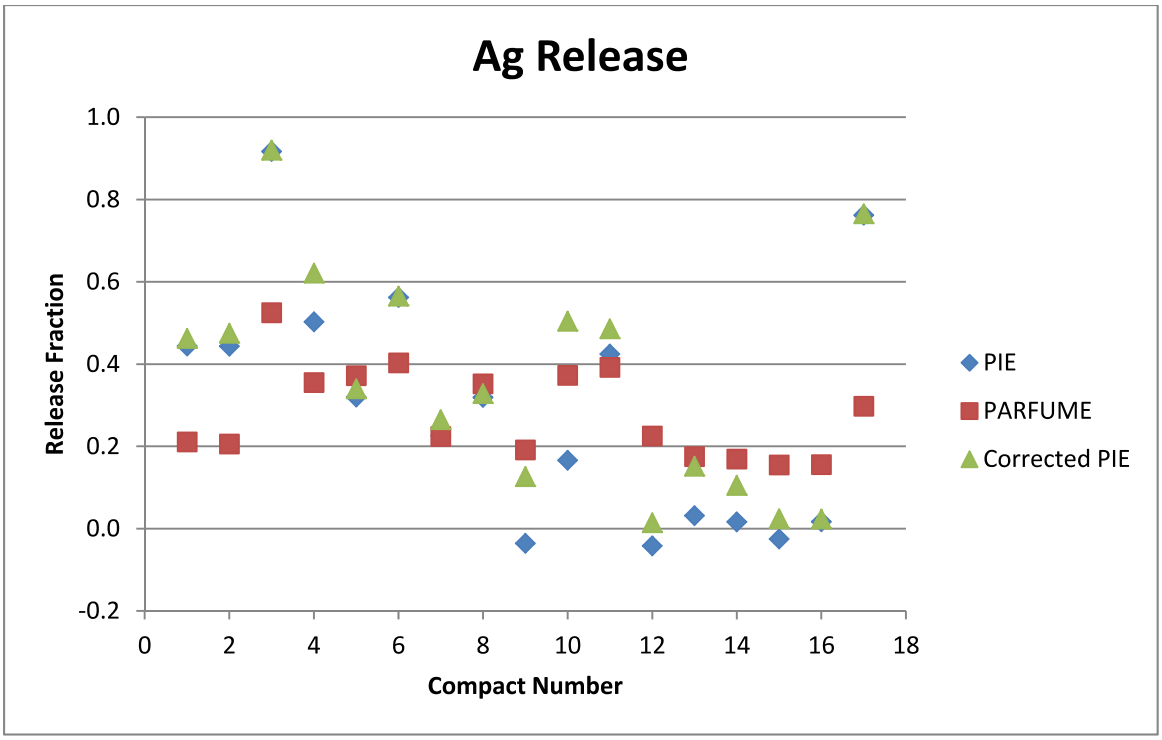

Figure 12. Compact (PIE) and particle (Corrected PIE) release compared to predicted PARFUME release (numbering follows order in Table 5).

Because of the high silver diffusivity in the graphite material, PARFUME does not predict any retention in the matrix, but AGR-1 PIE data show retention in the matrix can be significant. The complexity of the compacts' thermal histories mentioned in Section 3.2 does not allow correlating compact temperature and matrix content. Furthermore, the high matrix content of compacts 6-1-1, 4-4-3, 4-4-1, and 4-3-3 seems inconsistent with the lower content in the other compacts. Regardless, the PIE data suggest the matrix graphite material might be more retentive than initially expected and accounted for by modeling.

4.4 Discussion and Analysis on Silver Release

The silver release data inferred from compact gamma scanning and IMGA analysis of TRISO particles show the same trend when compared to PARFUME calculations: the model under-predicts the data in the bottom and top capsules and mostly overestimates silver release in the middle capsules.

4.4.1 Release vs. Temperature

As explained in Section 3.2, TAVA temperatures are not a suitable metric to correlate silver release to temperature because they do not adequately reflect the thermal state of the compacts throughout irradiation. Daily temperatures were therefore used to calculate the predicted silver release. In addition to their distribution around the compact TAVA temperature, the daily temperatures also widely vary spatially throughout a compact. As illustrated in Figure 13, daily temperatures can spread over several hundreds of degrees from the cold side to the hot side of a compact (Hawkes 2012), which can lead to a significant range in silver release from one particle to the other.

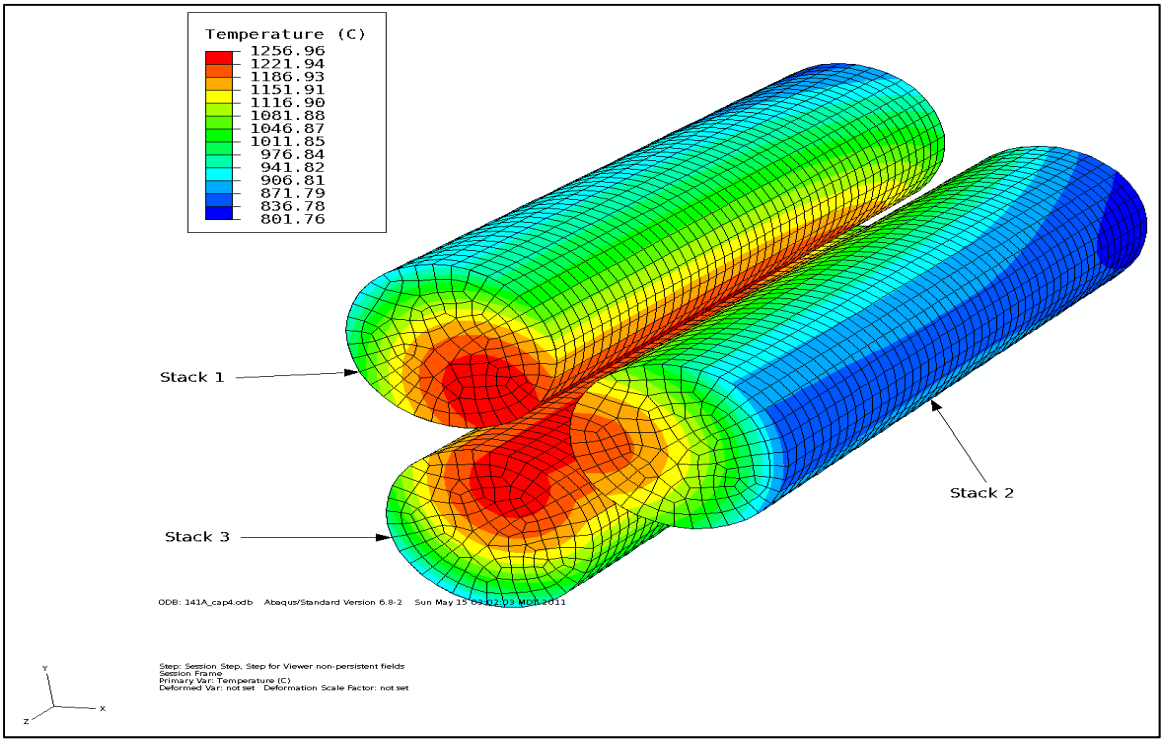

Figure 13. Temperature distribution across three stacks of compacts at mid-irradiation.

The temperature spatial distributions in the AGR-1 compacts were obtained from as-run thermal analysis (Hawkes 2012). Because of the large number of thermal nodes (roughly one node per particle), PARFUME could not be used to calculate the silver release of every single node. The predictions for silver release are based on the behavior of an average particle within each compact, whereas PIE measurements reflect the behavior of individual particles experiencing a broader set of daily temperatures because of their spatial locations all over the compact (in the case of compact gamma scanning) or at various locations whose daily temperatures might significantly differ from the compact average (in the case of IMGA).

To address the issue of spatial distribution and assess the impact of temperature distribution across a compact, an automated C-programmed scan through all the thermal nodes of Compact 6-3-2 was performed to determine the so-called "cold" and "hot" nodes of the compact. The diffusivity of silver in SiC was calculated for each node at every time step using the daily temperatures of that node, and the resulting diffusivities were summed to represent a time-integrated diffusivity in each node. Since the SiC layer is the main retention barrier for silver, this time-integrated diffusivity is a good indicator of silver release for that specific node. The "hot" node was then defined as the node with the highest time-integrated diffusivity, which is associated with a relative higher overall silver release. Conversely, the "cold" node was defined as the node with the smallest time-integrated diffusivity. PARFUME was then used to calculate the fractional release of silver for these two extreme nodes, using their respective daily temperatures and the compact average burnup and fast neutron fluence. Considering the large number of nodes used in the thermal calculations, it is approximated that one node is equivalent to one particle, even though the varying size of the thermal nodes makes it a rough approximation. PARFUME therefore treated the cold and hot nodes as cold and hot particles, calculating the fractional release at the outer edge of the OPyC layer.

Results were compared to the nominal fractional release of an average particle from Compact 6-3-2, obtained by averaging the daily temperatures of all the nodes (see average fractional release in Figure 11). The comparison between the nominal particle and the cold and hot particles is displayed in Figure 14. Figure 14 shows that particles from Compact 6-3-2 are predicted to release between 9% (cold particle) and 67% (hot particle) of their silver during irradiation, with a nominal value of 41%. The predicted release from Compact 6-3-2 is compared to PIE in Figure 15. Since IMGA measures the silver content of TRISO particles, Figure 15 displays the distribution of the retained fractions of silver rather than the release fractions. The PIE retained fraction is obtained by measuring the silver content and normalizing it by the silver inventory calculated by as-run neutronics. Because of the IMGA detection threshold, Figure 15 shows the distribution of particles with detectable silver and adds the contribution of particles for which the Ag-110m activity was below the detection limit (the detection limit was used as a conservative upper bound for the Ag-110m activity). For Compact 6-3-2, the distribution of retained silver spans from 8 to 88%, which encompasses almost all of the predicted range of 33 to 91%? The agreement between PARFUME and PIE is not as close on Compact 1-3-1 for which the measured and predicted ranges are displayed in Figure 16. The IMGA distribution ranges from 6 to 53%, while the PARFUME prediction ranges from 64 to 98%, showing a significant offset although the widths of both ranges are somewhat comparable.

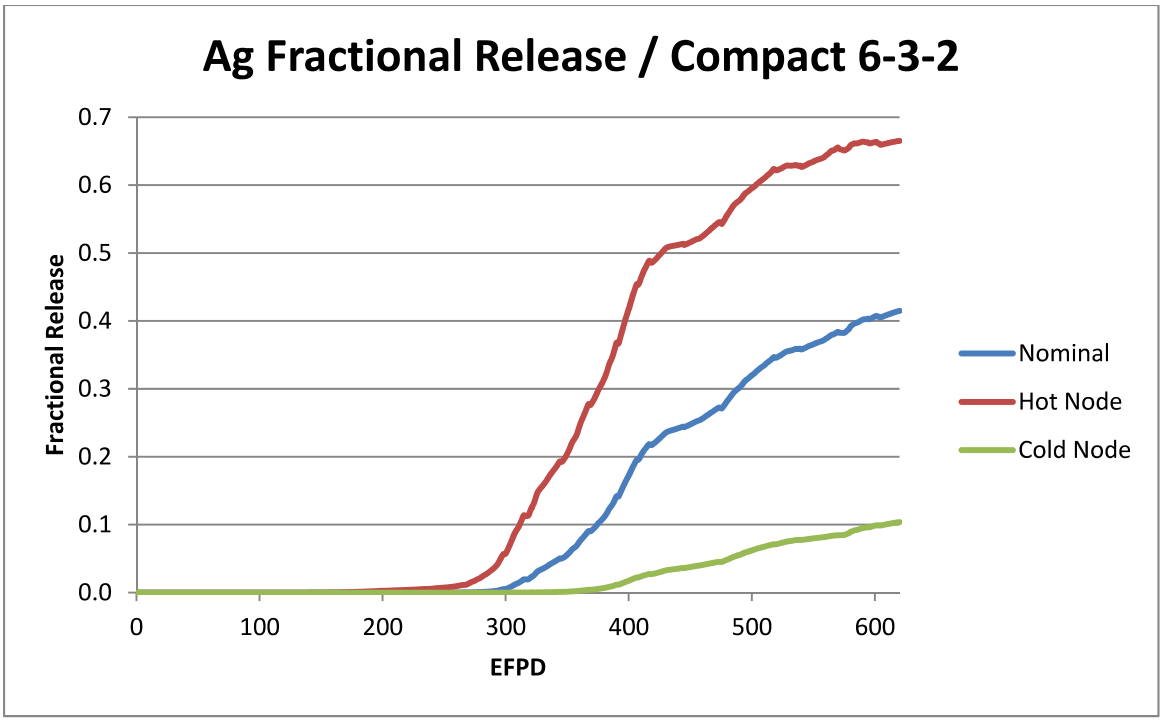

Figure 14. Silver fractional release for cold and hot particles in Compact 6-3-2 during the AGR-1 irradiation.

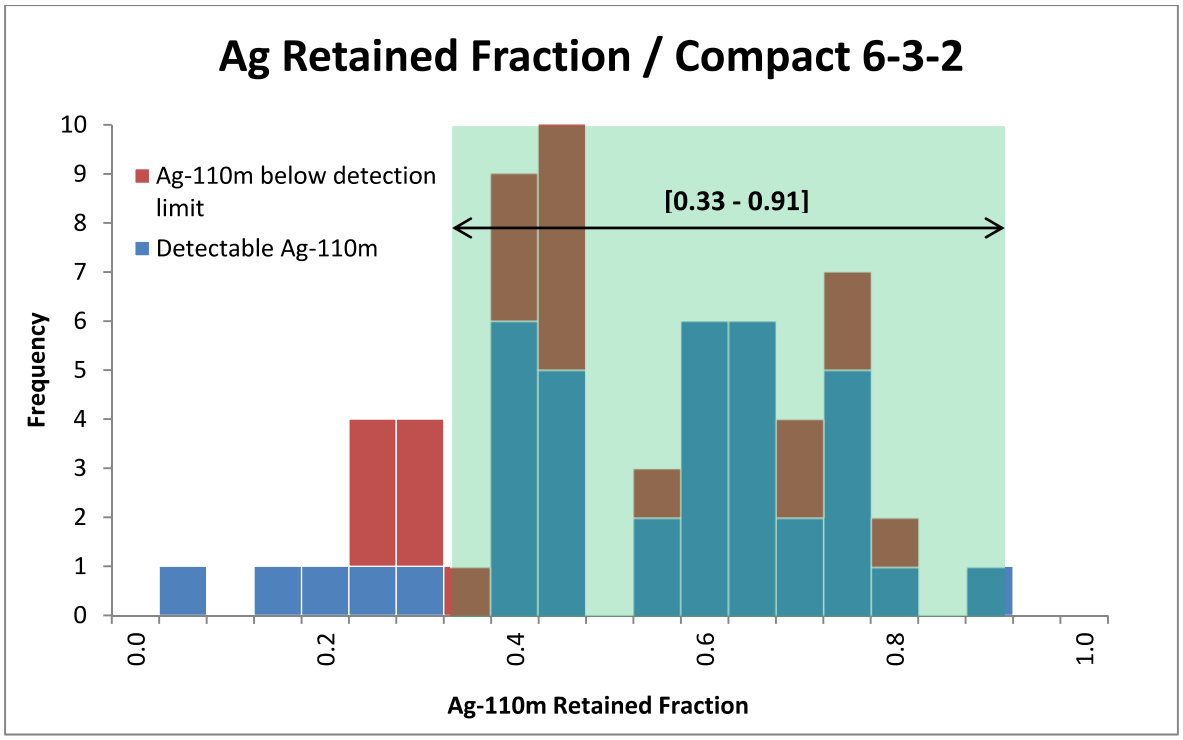

Figure 15. Silver retained fraction of 60 randomly selected particles from Compact 6-3-2 compared to the range of values predicted by PARFUME.

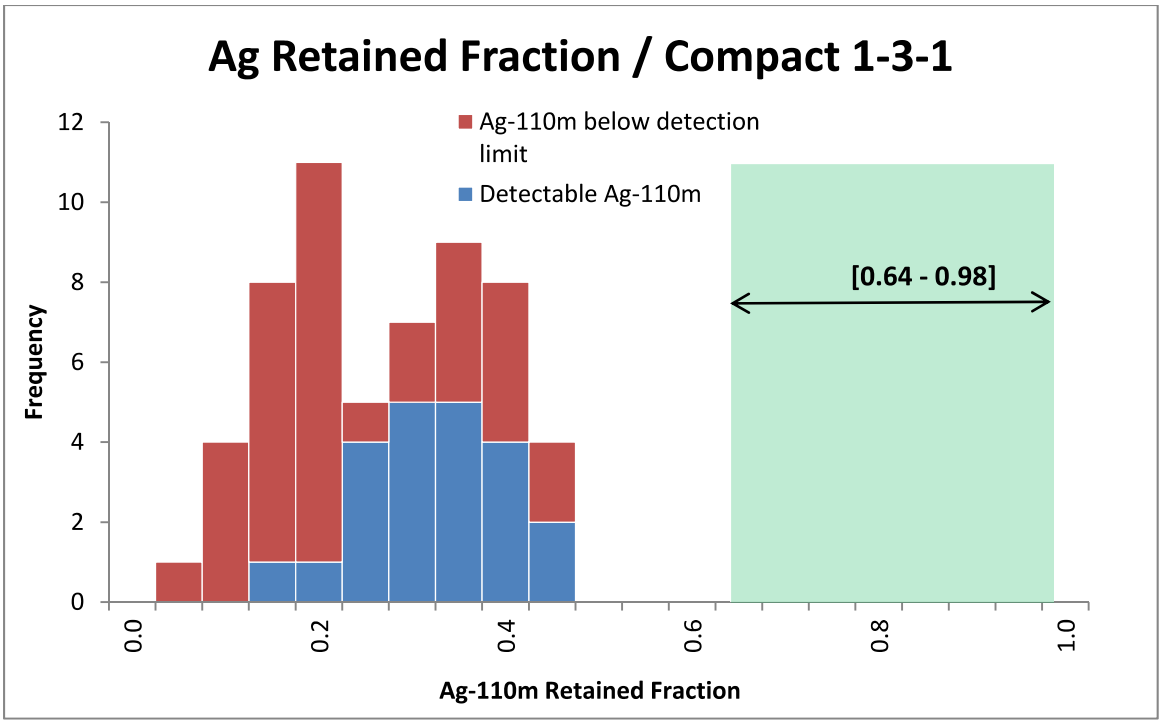

Figure 16. Silver retained fraction of 60 randomly selected particles from Compact 1-3-1 compared to the range of values predicted by PARFUME.

The discrepancy observed between PARFUME and PIE when comparing the average fractional release (or retained fraction) can be largely attributed to the wide distribution of temperatures experienced by a compact during irradiation. PARFUME uses the volume-average daily temperatures to compute the average fractional release for each compact, while IMGA measurements are performed on a subset of particles whose exact irradiation history is not because information regarding the original location of the particles in the compact was lost during the deconsolidation. Furthermore, in the case of PARFUME, the release fraction of a particle bearing the volume-average daily temperatures is not equivalent to the average of the release fractions of all individual particles in the compact because the diffusivity does not vary linearly with temperature (see Section 3.4). Therefore, using the volume-average daily temperatures underestimates the release by neglecting the relatively larger release of hotter particles. This also causes a discrepancy between PARFUME and PIE when comparing fractional release from compact gamma scanning.

As-run calculations report uncertainties on the calculated temperatures up to 100°C (Collin 2014). Although no temperature bias was reported, Figure 17 shows the impact of a temperature change on the silver release calculated by PARFUME. Compacts in Figure 17 are numbered in the order presented in Table 1. For each of the 56 gamma scanned compacts, the temperature was roughly adjusted in PARFUME calculations to attempt to match the PIE release. For instance, the daily temperatures of Compact 6-2-3 (first from the left) were increased by +200°C so the resulting calculated release fraction would more closely match the measured release fraction of the compact, the increase was +50°C for Compact 6-1-3 (second from the left), and so forth. Figure 17 displays the PIE data and the original PARFUME predictions together with the release predictions obtained after the temperature changes. Consequently, each compact is attributed three data points: PIE release fraction, initial PARFUME release fraction, and temperature-adjusted PARFUME release fraction. In the case no temperature adjustment was needed, there are only two data points displayed (PIE and initial PARFUME release fractions). The minimum temperature change was limited to -100°C as PARFUME cannot calculate negative release fractions as assessed by PIE. Figure 17 shows the PARFUME/PIE comparison can be significantly improved by a reasonable temperature adjustment. The reason is that at the AGR-1 temperatures, the diffusion is very sensitive to even a small temperature change due to the exponential shape of the diffusion coefficients.

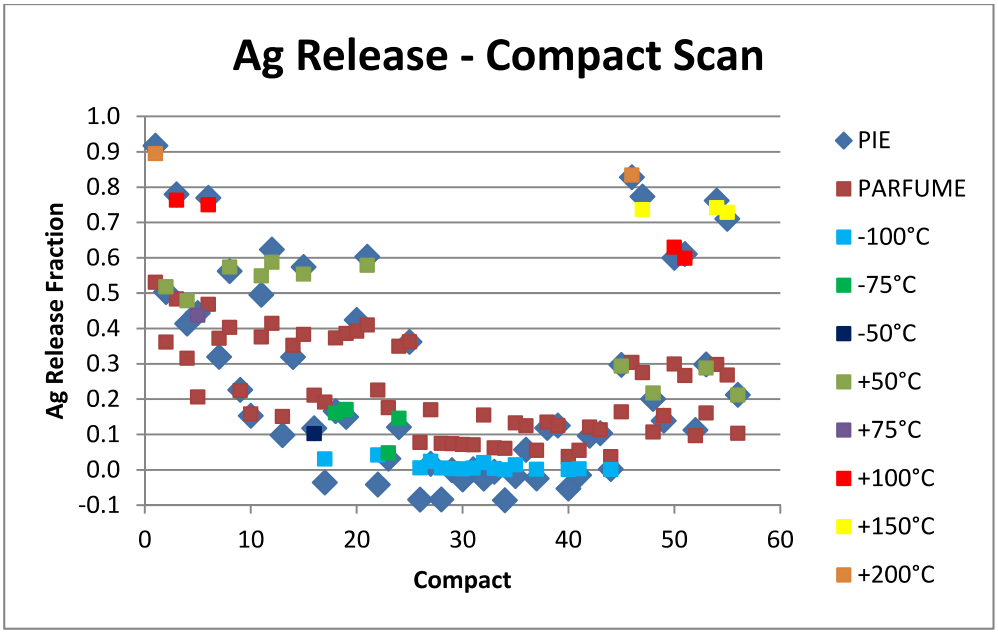

Figure 17. Effect of temperature adjustment on calculated silver release (numbering follows the order in Table 1).

Table 6 gives a summary of the impact of temperature change on silver release. The table shows the average absolute and relative variations of the release fractions as a function of the temperature variation in the compacts. For each temperature adjustment, Table 6 shows the range of the initial PARFUME release fractions for the compacts affected by that temperature adjustment (Compacts 6-2-3 and 1-3-3 for a temperature adjustment of +200°C, for instance), and the range of release fractions calculated by PARFUME after the temperature adjustment. Because of the broad distribution of the release fractions amongst all compacts, some large relative variations can be associated with small absolute variations. The table shows that the sensitivity of release to temperature is rather large.

Table 6. Effect of temperature adjustment on calculated silver release.

Temperature adjustment	Initial release fraction range	Temperature-adjusted release fraction range	Absolute variation range	Relative variation range
-100°C	$3.7\times10^{-2} - 2.3\times10^{-1}$	$2.0\times10^{-4} - 4.2\times10^{-2}$	[-0.18, -0.04]	[-100%, -82%]
-75°C	$1.8\times10^{-1} - 3.9\times10^{-1}$	$4.8\times10^{-2} - 1.7\times10^{-1}$	[-0.22, -0.13]	[-73%, -56%]
-50°C	$1.2\times10^{-1} - 3.9\times10^{-1}$	$4.9\times10^{-2} - 2.3\times10^{-1}$	[-0.15, -0.08]	[-61%, -40%]
+50°C	$1.0\times10^{-1} - 4.1\times10^{-1}$	$2.1\times10^{-1} - 5.9\times10^{-1}$	[0.11, 0.15]	[41%, 105%]
+75°C	2.1×10^{-1}	4.4×10^{-1}	0.23	113%
+100°C	$2.7\times10^{-1} - 4.8\times10^{-1}$	$6.0\times10^{-1} - 7.6\times10^{-1}$	[0.28, 0.33]	[58%, 125%]
+150°C	$2.7\times10^{-1} - 3.0\times10^{-1}$	$7.3\times10^{-1} - 7.4\times10^{-1}$	[0.44, 0.46]	[149%, 172%]
+200°C	$3.0\times10^{-1} - 5.3\times10^{-1}$	$8.3\times10^{-1} - 8.9\times10^{-1}$	[0.36, 0.53]	[69%, 175%]

In addition, Table 7 shows the repartition of the temperature adjustments by capsule. It shows the higher adjustments where needed for Capsules 1 and 6, and the lowest adjustments for Capsules 2, 3, and 4. Most of the -100°C adjustments were meant to match PIE release fractions lower than 2%, or even negative (which PARFUME cannot compute). Considering PARFUME overpredicts PIE release in the middle capsules and overpredicts PIE in the top and bottom capsules (see Figure 10), the results shown in Table 7 are consistent with the previous conclusion.

Table 7. Temperature adjustment by capsule.

Capsule	-100°C	-75°C	-50°C	No change	+50°C	+75°C	+100°C	+150°C	+200°C	Total
6	-	-	-	-	2	1	2	-	1	*6*
5	-	-	1	5	4	-	-	-	-	*10*
4	2	4	-	2	1	-	-	-	-	*9*
3	8	-	-	-	-	-	-	-	-	*8*
2	6	-	-	5	-	-	-	-	-	*11*
1	-	-	-	2	4	-	2	3	1	*12*
Total	*16*	*4*	*1*	*14*	*11*	*1*	*4*	*3*	*2*	*56*

4.4.2 Release vs. Burnup

Appendix C shows plots of the measured and calculated silver fractional release as a function of burnup, fast fluence, and TAVA temperature. As explained in Section 3.2, TAVA temperatures are not a good metric to correlate silver release to irradiation temperature. On the other hand, a slight correlation between silver fractional release and burnup can be observed in the related plot in Appendix C, but this correlation might be an indirect effect of the temperature-dependence of the silver release.

The decrease of the silver fractional release with burnup can be partially explained by the plot displayed in Figure 18. The plot shows the correlation between burnup and the TAVA temperatures calculated over the full 620 days of irradiation and calculated over the last 310 days of irradiation. Figure 18 shows the temperature in the compacts globally was higher in the second half of the irradiation compared to the first half, though some compacts experienced some of their higher daily temperatures during the first half of irradiation, as can be seen in Figure 5 for Compact 4-4-1 (see Section 3.2). The TAVA temperature of each compact encompasses the low temperatures experienced early during irradiation. Computing the TAVA temperatures for only the second half of irradiation gives an indication on how hot the compacts were towards the end of irradiation.

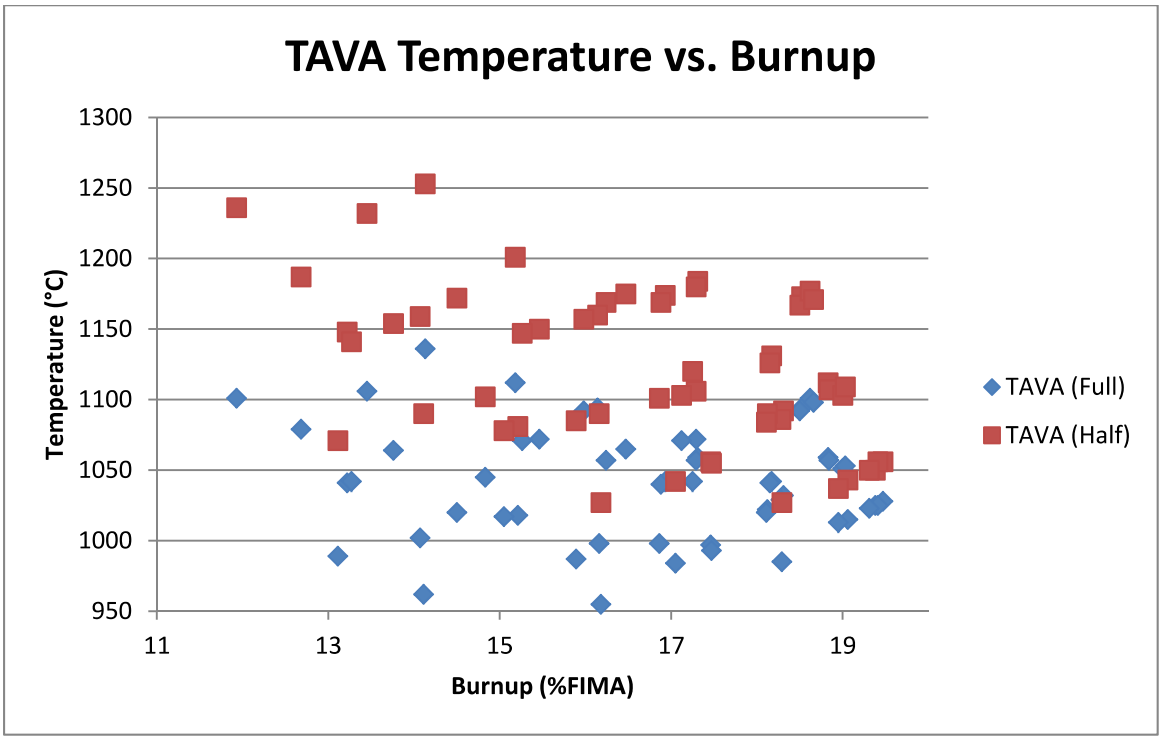

Figure 18. Correlation between burnup and TAVA temperatures calculated for the full irradiation and for the second half of irradiation.

Figure 18 shows the lower burnup compacts experienced the larger temperature differences between the first and second halves of irradiation, and they also tended to have higher temperatures during the second half of irradiation, yielding higher TAVA temperatures ("TAVA (Half)" data on Figure 18). This is easily explained by considering that the lower burnup compacts had more fissile material inventory towards the end of irradiation than higher burnup compacts, and they therefore had higher fission rates which ultimately led to higher heat generation rates and, consequently, higher temperatures.

The larger release of silver is obtained when high temperatures force the diffusion of a large amount of silver through the TRISO particle. This is typically the case towards the end of irradiation, when the silver source has accumulated significantly with time, and only if the temperature of the compact is high enough. Figure 5 shows that, early during irradiation, the amount of silver produced in the kernel is limited. Consequently, for compacts with high temperatures early during irradiation, the silver production was not significant enough through the first half of irradiation to be released in large quantities. To a good approximation, it can therefore be considered most of the significant release occurred late in the irradiation. As seen in Figure 18, compacts with lower burnup became hotter towards the end of irradiation, which explains the higher fractional release for low burnup compacts as observed in Appendix C and in PIE.

As an illustration, Figure 5 shows that Compacts 4-4-1 and 4-3-2 both have a TAVA temperature of 1057°C, but Compact 4-3-2 got hotter towards the end of irradiation. This is confirmed by the TAVA temperatures calculated over the second half of irradiation, with Compact 4-4-1 having a resulting TAVA temperature of 1107°C compared to 1169°C for Compact 4-3-2. As discussed in Section 3.2, Compact 4-3-2 yielded the higher silver release because its daily temperature was higher towards the end of irradiation.

Figure 19 shows the difference in release fractions between PARFUME and PIE measurements as a function of burnup. A slight trend can be drawn in the observed under-prediction at low burnup and overprediction at high burnup. As seen in Appendix C, both PIE data and PARFUME exhibit the trend of a higher release at low burnup, but the trend seems more marked in the case of PIE measurements. The issue of temperature spatial distribution discussed above can possibly explain the observed trend but a direct burnup effect not captured by PARFUME cannot be ruled out.

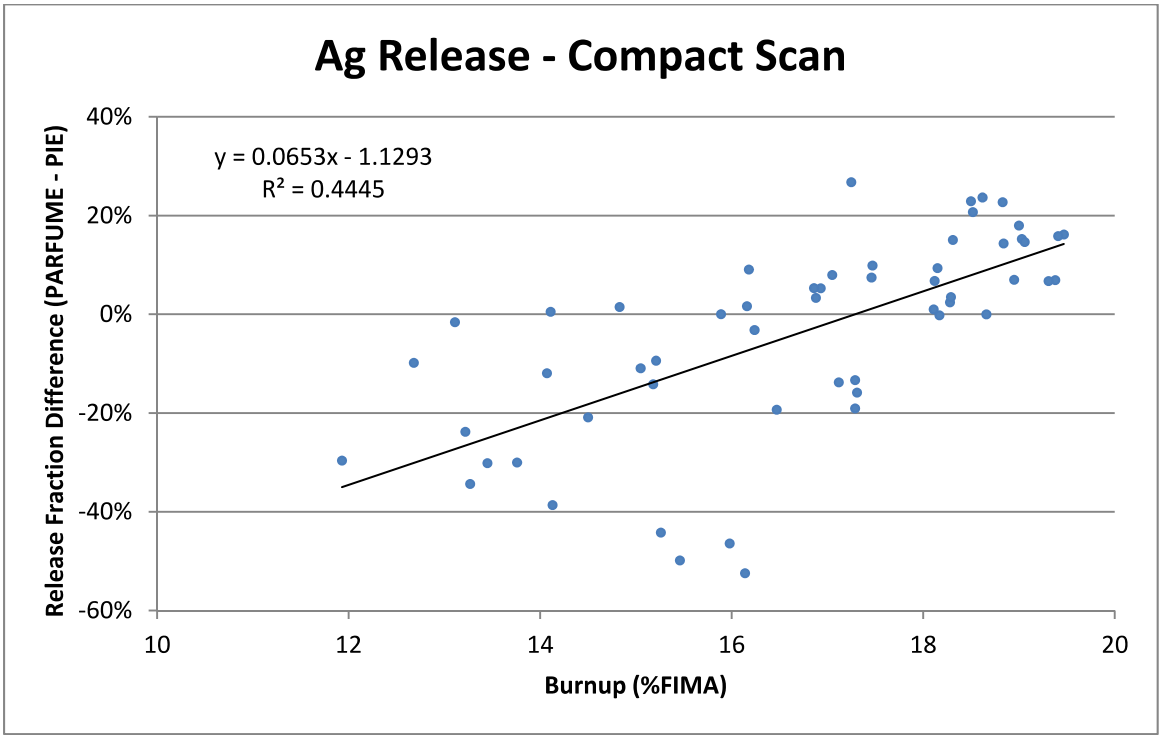

Figure 19. Silver fractional release difference between PARFUME and PIE versus burnup.

4.4.3 Release versus Source

The release of silver is primarily driven by temperature. Section 4.4.2 showed there is some uncertainty in the prediction of silver release because of the temperature spatial distribution across the compacts. The silver source is also spatially distributed across the compact, but both the PARFUME calculations and the release fractions calculated from the PIE measurements consider a uniform source averaged over the compact volume to normalize the amount of released silver. In reality, the silver source is directly linked to the distributions of neutron flux and fission density within a compact. The neutron flux was not uniform throughout the capsules, as there are both axial and azimuthal variations. Consequently, a gradient in fission density rate existed throughout the capsules and within each individual compact, as illustrated in Figure 20 for Compact 3-2-1. This resulted in a variation in the relative amounts of uranium 235 (U-235) and plutonium 239 (Pu-239) in the compacts, and therefore the subsequent Ag-109 production and activation to Ag-110m were not uniform throughout the compacts, leading to a distribution of the Ag-110m source across the compacts.

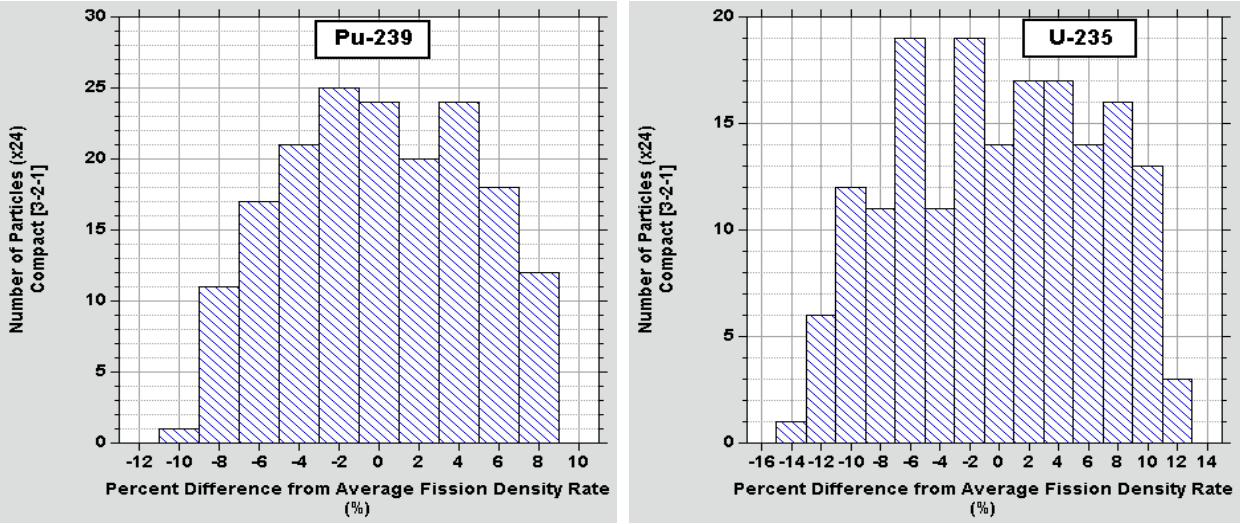

Figure 20. Distribution of fission density rates across Compact 3-2-1.

Because of the time-consuming calculations needed to predict the fission product source of each of the 4,000+ particles per compact, both PARFUME and as-run neutronics used average sources. In PARFUME, the source is at the particle level and it is obtained by calculating the source of an average particle bearing the average burnup of the compact. The silver fission yield used in this calculation is expressed as a burnup-dependent correlation obtained from a coupled calculation between MCNP (LANL 2004) and ORIGEN2 (Croff 1983) that takes into account the production of Ag-109 from uranium and plutonium fission, and the subsequent activation to Ag-110m. The as-run neutronics calculation of the source is done directly at the compact level. The two sources are related by the number of particles in the compact. Figure 21 shows the normalized silver sources as a function of burnup for a randomly chosen compact (Compact 3-4-3), as calculated by PARFUME and as-run neutronics. In both cases, the relative magnitude of the source has no impact when calculating the release fractions because of the very definition of the release fraction that normalizes the release to the source term.

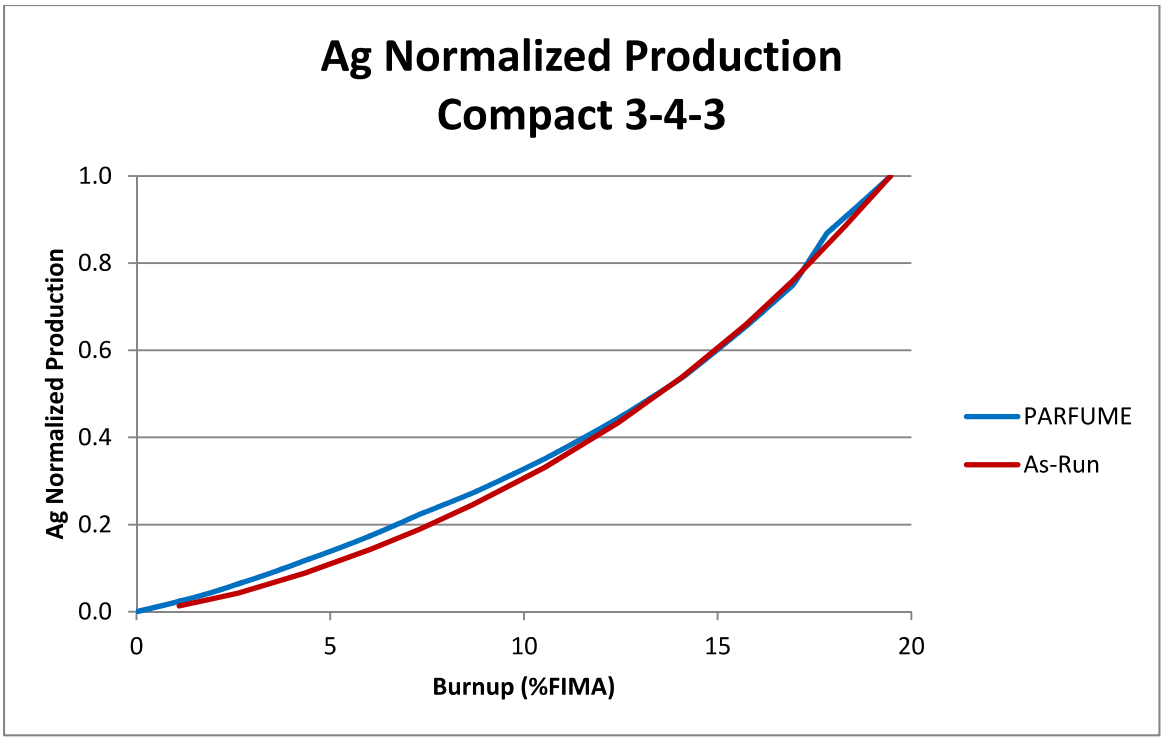

Figure 21. Silver normalized source as a function of burnup for Compact 3-4-3.

The first consequence of using average sources is that these calculated average sources are not equal to the real silver source produced during irradiation. Because the effective fission product yield of silver (which takes into account production from both U-235 and Pu-239) is not independent of burnup, the silver source exhibits a non-linear build-up with time. This non-linearity implies the source obtained at the average compact burnup (calculated sources) is not equal to the average source obtained from all the sources of the individual particles, each at their own burnup (real source). Appendix D offers a detailed theoretical explanation as to why the two calculated sources do not represent the real source, and therefore only allow estimates of the real fractional release of the irradiated compacts. Furthermore, even though PIE and PARFUME use a similar source to normalize their respective measured or calculated release, Appendix D shows that PIE and PARFUME results cannot provide comparable silver release fractions independently of the temperature issue. This is again due to the non-linearity of the silver generation rate with burnup.

PARFUME calculates the fractional release of silver independently of its isotopes. This is because the effective fission product yield used for silver does not discriminate its isotopes but was calculated to reflect the overall production of silver with burnup. In the case of PIE, the release of isotope Ag-110m is measured, and Figure 22 shows that its production by activation of isotope Ag-109 is shifted in time. Anyhow, the release fraction of Ag-110m is the same as the release fraction of Ag-109 if it is assumed that (a) both isotopes are similarly distributed across the compacts, and (b) both isotopes behave similarly in regard to diffusion through the TRISO particles and matrix. The second assumption seems reasonable but it cannot be confirmed by any experimental data or backed-up by any theoretical diffusion model. It also cannot be modeled by PARFUME since the code does not differentiate between isotopes. That assumption also entails that the variation in time of the Ag-110m/Ag-109 ratio, as illustrated on Figure 22, has no impact on their respective release fractions: both release fractions are equal because of the similar diffusion behavior of the two isotopes, and because the relative magnitude of the source does not modify the subsequent release fraction. The first assumption, on the other hand, is dubious at best since the neutron flux is not spatially uniform across a given compact, resulting in non-uniform

distributions of Ag-109 and Ag-110m across that compact, as explained previously. Because Ag-110m is produced by activation of Ag-109, the effect of a non-uniform neutron flux on the Ag-110m distribution is amplified. Since particles are not individually modeled by as-run neutronics or by PARFUME, these non-uniformities of the Ag-109 and Ag-110m distributions are not captured by calculation. Therefore, their impact on the measured and calculated release fractions of silver cannot be properly assessed.

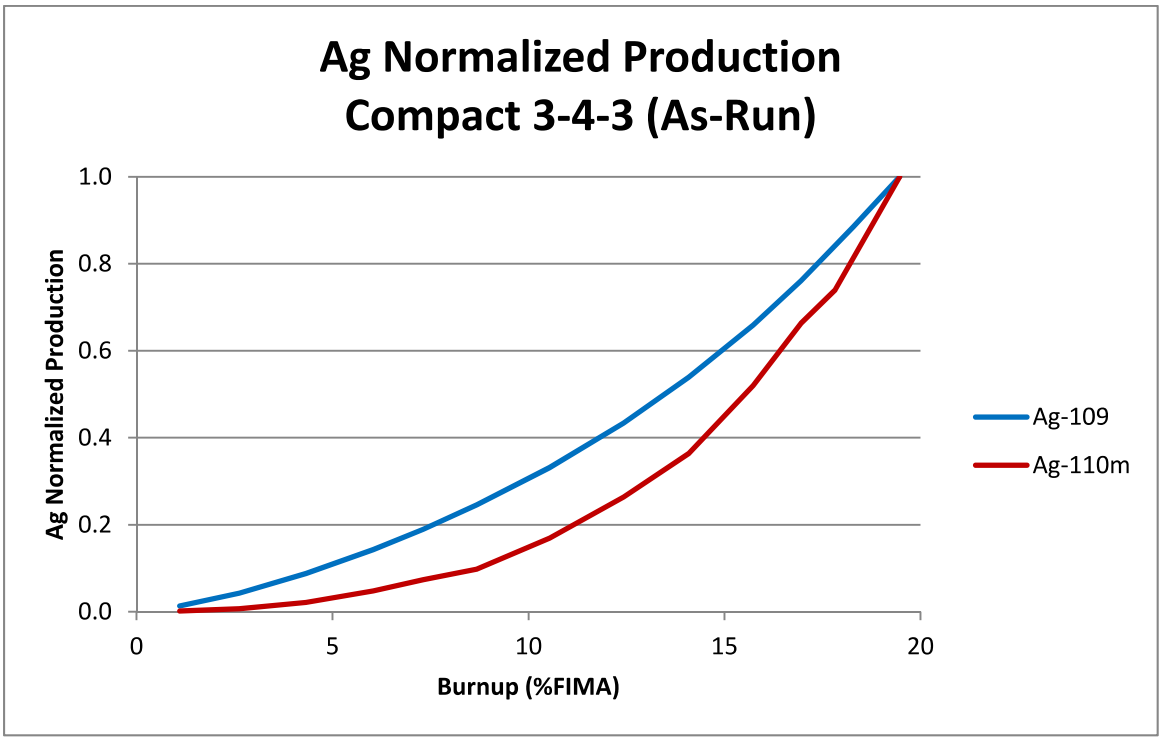

Figure 22. Ag-109 and Ag-110m normalized sources as a function of burnup for Compact 3-4-3.

4.4.4 Summary

As a consequence of the temperature and burnup spatial distributions across the compacts, the comparison between PARFUME calculations and PIE measurements is not straightforward. There are major factors affecting both the data and calculations used in this fractional release assessment, namely:

- Accuracy of the silver diffusivities (PARFUME)
- Accuracy of the predicted compact temperatures (PARFUME)
- Spatial distribution of the compact daily temperatures (PARFUME)
- Spatial distribution of the silver source (PARFUME)
- Uncertainty from gamma scanning measurements (PIE)
- Predicted Ag-110m activity (PIE).

Nevertheless, PARFUME predictions and PIE measurements are in reasonably good agreement, and PARFUME was able to explain the large distribution in silver release from IMGA measurements by pointing out and demonstrating the temperature spatial distribution issue.

It also appears likely that low burnup capsules tend to have a higher silver release because they became hotter towards the end of irradiation when silver was readily available for release. Comparisons also show a trend of PARFUME under-predicting PIE data in the lower burnup capsules and overpredicting PIE data in the higher burnup capsules. The simplified modeling, that does not take into account the spatial distribution of the temperature across the compacts, partially explains the trend but a definitive answer could not be achieved without more modeling efforts. Refined computing with spatial burnup and temperature distributions would allow better predictions of the fractional release of silver and a more accurate comparison of the model predictions to compact gamma scanning results. On the contrary, the difficulty of selecting individual particles based on their original location in a compact would not allow any better comparison to IMGA results.

Comparing PIE data and PARFUME predictions also brought to light that the matrix graphite material is more retentive than expected, as silver is found outside the SiC layer by PIE, while PARFUME predicts no appreciable retention.

5. CESIUM AND STRONTIUM RELEASE

5.1 Deconsolidation-Leach-Burn-Leach

DLBL was performed on the nine compacts listed in Table 2 (see Section 2). For compacts containing all intact particles, the DLBL measurement includes the contribution from the amount of fission products released through intact coatings but retained in the compact outside of the SiC layer, as well as fission products from uranium contamination in the OPyC and the compact matrix. As mentioned in Section 2, the uranium contamination in AGR-1compacts was on average lower than 4×10^{-7} for each fuel variant, so any release significantly above this level can be assumed to come from other sources.

The DLBL data therefore represents a partial inventory of fission products released from intact particles, as it does not account for fission products released from the compacts and found on capsule components. If any particles with failed SiC are present—and the particles are not removed from the population before the burn-leach is performed—then the inventory of the kernels from these particles will also be included in the post-burn leach solutions, and may greatly exceed the level of fission products attributed to diffusive release through coatings.

Based on analysis of fission products in the capsule components (Harp 2012), it was determined that compacts 6-3-2, 5-2-3, and 5-2-1 may have one or more particles with a non-retentive SiC layer. DLBL results from Compact 6-3-2 indicated the presence of one such particle, the kernel of which was dissolved during post-burn leaching (and therefore the DLBL totals include the contribution from this kernel). Gamma analysis of particles from Compact 5-2-3 revealed that this compact contained two such particles. Compact 5-2-1 was determined to have one such particle. In both cases, these particles were removed from the population before DLBL analysis, and so the remaining inventory in the kernels was not dissolved during the DLBL process (Hunn 2014).

Two sets of calculations were performed with PARFUME. The first set calculates the diffusive release from compacts containing intact particles only. The second set calculates the diffusive release from compacts containing one or two particles with failed IPyC and SiC layers, in order to model the compacts that PIE determined to have leaking particles. Because PIE measurements indicate very little cesium release from intact particles, the second set of calculations assumes no diffusion of cesium from intact particles in order to compare PARFUME predictions of release from particles with failed SiC to PIE measurements. However, PIE data indicate a non-negligible strontium release from intact particles. Thus all strontium calculations account for strontium released by intact particles because their contribution is not negligible when compared to the amount of strontium released by the particles with failed SiC. This allows for modeling results to attempt to more closely match PIE measurements.

For each compact, the PIE measurements were corrected to take into account the amount of cesium and strontium released from the compacts and collected on the capsule components (e.g., primarily the graphite holder and stainless steel shell). In each capsule, the fraction of cesium or strontium deposited on the capsule components cannot be easily attributed to the specific compact from which it originated. Therefore, an assumption had to be made for each capsule when taking into account the amount of cesium or strontium that was transported beyond the compacts. This assumption leads to different cases:

- Capsules 1 to 4. These capsules contain compacts with intact particles only. In this case, a lower bound assumes none of the cesium and strontium found on the capsule components originates from the analyzed compact (label “DLBL Min” in Figures 23–26). On the other hand, an upper bound assumes that all of the cesium or strontium found on the capsule components originates from the analyzed compact (“DLBL Max”).

- Capsule 5. PIE data from Capsule 5 includes two compacts (5-2-3 and 5-2-1) with non-retentive particles (the only two compacts in the capsule with non-retentive particles), and one compact (5-3-1) with intact particles only. The non-retentive particles were screened out by IMGA prior to post-burn leach, which means that the cesium and strontium contained in the kernels of these non-retentive particles were not part of the post-burn leach solutions. The DLBL results combined with the inventory on the capsule components therefore directly give access to the release of these non-retentive particles.
  - In the case of cesium, PIE analysis indicates that the majority of the cesium found in the capsule components originated from the non-retentive particles, so there is therefore no "DLBL Min" value attributed to cesium release for Compacts 5-2-3 and 5-2-1 (i.e., it is not credible to assume that none of the inventory on the capsule components came from these two compacts, when in fact the data indicate most of it did). Conversely, the intact particles have a low cesium release and their contribution to the inventory on the capsule components is negligible. There is therefore no "DLBL Max" value attributed to Compact 5-3-1 (i.e., it is not credible to assume that most of the cesium on the capsule components came from Compact 5-3-1, since the data indicate that it mostly came from Compacts 5-2-3 and 5-2-1).
  - In the case of strontium, the release from intact particles is significant, so the total capsule fraction on the capsule components is assumed to have been released equally from all twelve compacts (i.e., the release fraction from all 12 compacts is the same). Anyhow, the inventory on the capsule components is small relative to the inventory in the compact matrices, so the lower and upper bounds are essentially similar.
- Capsule 6: PIE data for Capsule 6 includes one compact (6-3-2) with one non-retentive particle (the only compact in the capsule with any non-retentive particles), and one compact (6-1-1) with intact particles only. The kernel inside the non-retentive particle of Compact 6-3-2 was leached in the post-burn leach solutions, so the total DLBL inventory includes cesium and strontium that were retained in the matrix as well as in the exposed kernel.
  - In the case of cesium, uranium measurement indicates the pre-burn leach of Compact 6-3-2 contained none of the kernel, and therefore represents only cesium from the matrix. The post-burn leach could contain residual cesium from the compact outside the SiC layer, but it is assumed for the purposes of this analysis the cesium inventory comes predominantly from the exposed kernel. As a first approximation, the pre-burn leach data is therefore used as the estimate of the cesium inventory in the compact outside the SiC layer. As was the case with Capsule 5, the majority of the cesium found in the capsule components originated from the non-retentive particle of Compact 6-3-2, therefore no "DLBL Min" is attributed to that compact, and no "DLBL Max" value is attributed to Compact 6-1-1.
  - In the case of strontium, it is not possible to determine how much strontium was retained in the kernel of Compact 6-3-2 from the analysis of the leach solutions. The total Sr-90 inventory in the DLBL solutions was equivalent to the inventory in approximately two particles; however, because the inventory typically found outside of the SiC layer of intact particles is often of a similar order of magnitude, the relative contribution from the single exposed kernel cannot be separated from the contribution from the remaining intact particles. Two assumptions were then made to set up lower and upper boundaries to the strontium release. The first assumption considers full kernel retention of the strontium and equates the inventory of the pre-burn leach to the strontium released during normal irradiation ("DLBL Min"). The second assumption considers that the strontium was not retained by the kernel, in which case the inventory of both the pre-burn and post-burn leaches gives an upper limit on the strontium release in Compact 6-3-2 ("DLBL Max"). In addition, the inventory on the capsule components was treated similarly as in Capsule 5. The contribution from intact particles is minor and it essentially does not affect the measured strontium release.

These cases are displayed in Figures 23 through 26. In these figures, “PARF Intact” represents the calculated release fractions of compacts containing intact particles only, and “PARF N Fail” represents the calculated release fractions of compacts containing N particles (N = 1 or 2) with failed SiC layers. Because of the measured amount of release from intact particles, the contribution from intact particles is either included (case of Sr, for which the release from intact particles is not negligible), or excluded (case of Cs, for which intact particles barely release) from the calculated release fractions of compacts containing particles with failed SiC layers. Therefore, in the case of cesium, PARF N Fail excludes the contribution from intact particles, and only represents the calculated release from the particles with failed SiC, and, in the case of strontium, PARF N Fail represents the sum of the calculated release from intact particles and from particles with failed SiC. PARF Intact is also displayed in the figures corresponding to compacts containing particles with failed SiC to separately show the calculated contribution from the intact particles.

The measured fractional release of cesium from intact particles can vary by up to two orders of magnitude between the compacts displayed in Figure 23, whereas the release of strontium is even more scattered, ranging over three orders of magnitude, as can be seen in Figure 25.

The levels of fractional release for cesium measured by PIE and shown in Figures 23 and 24 indicate the release of cesium is dominated by particles with failed SiC, and intact particles barely release any of their cesium. On the other hand, Figure 25 shows, in some cases, the release of strontium from intact particles is not negligible. Looking at Figure 26, it is difficult to conclude if the strontium release from Compacts 5-2-1, 5-2-3, and 6-3-2 is dominated by few the particles with failed SiC or by the bulk of intact particles.

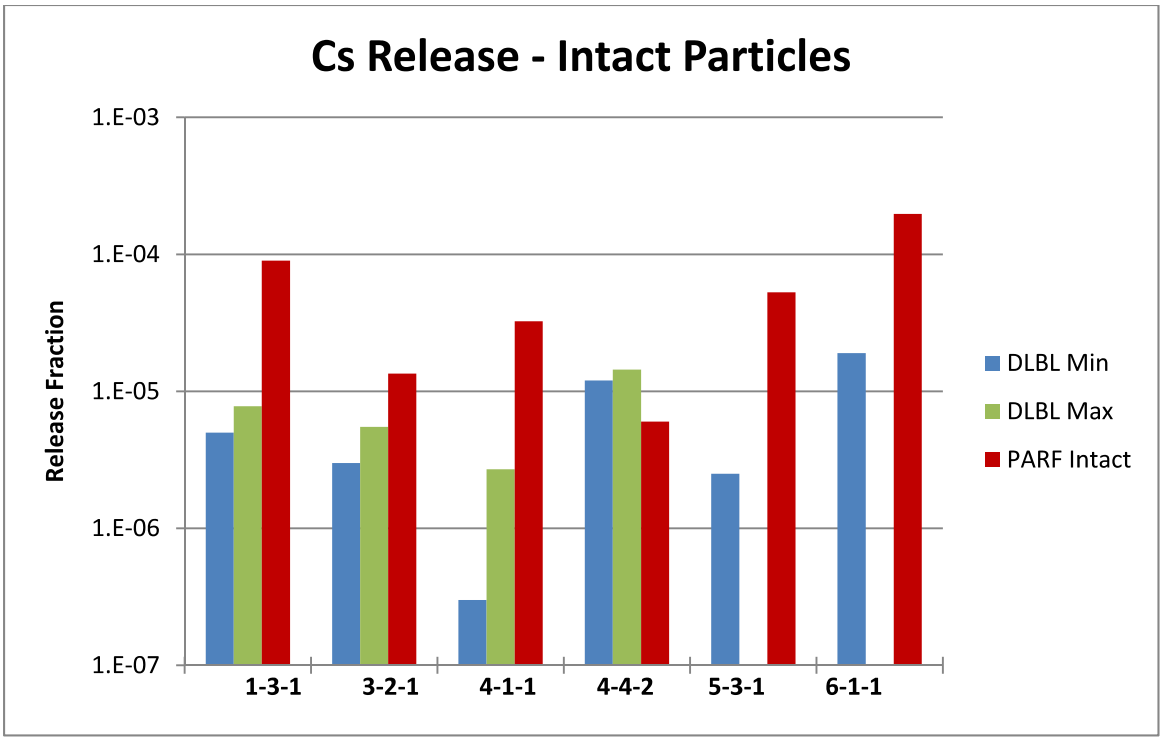

Figure 23. Cesium fractional release from compacts containing intact particles only.

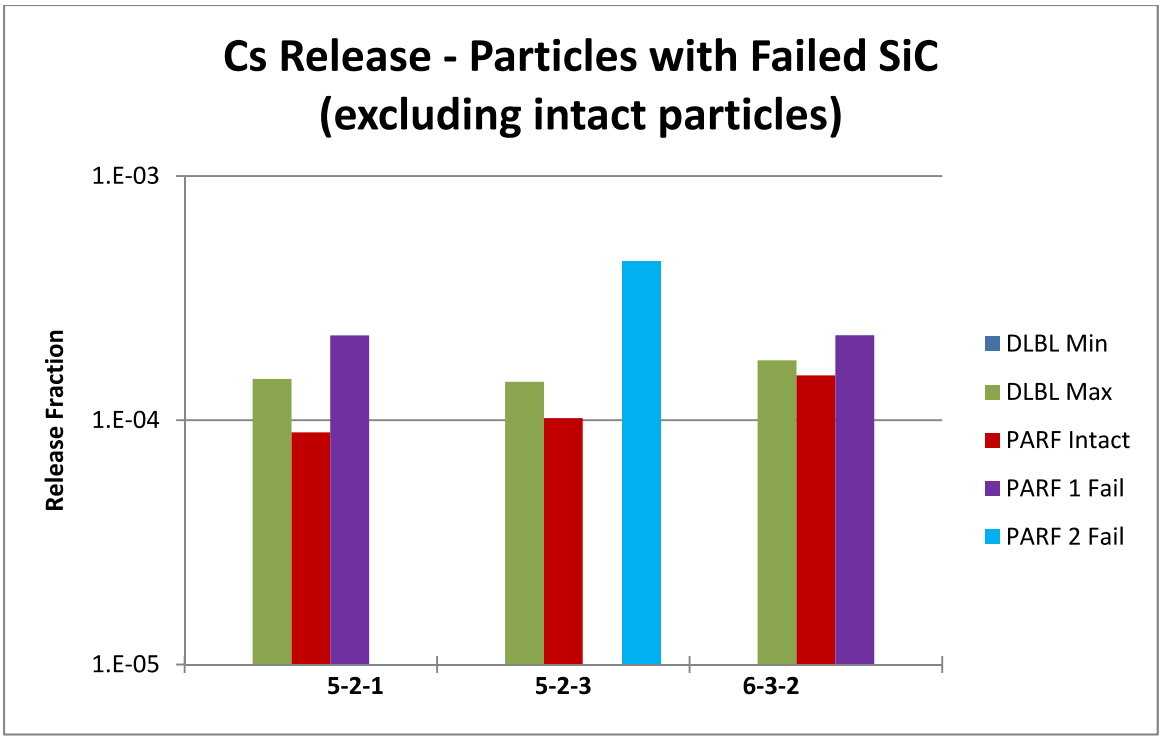

Figure 24. Cesium fractional release from compacts containing particles with failed SiC layers. PARFUME predictions exclude the release from intact particles.

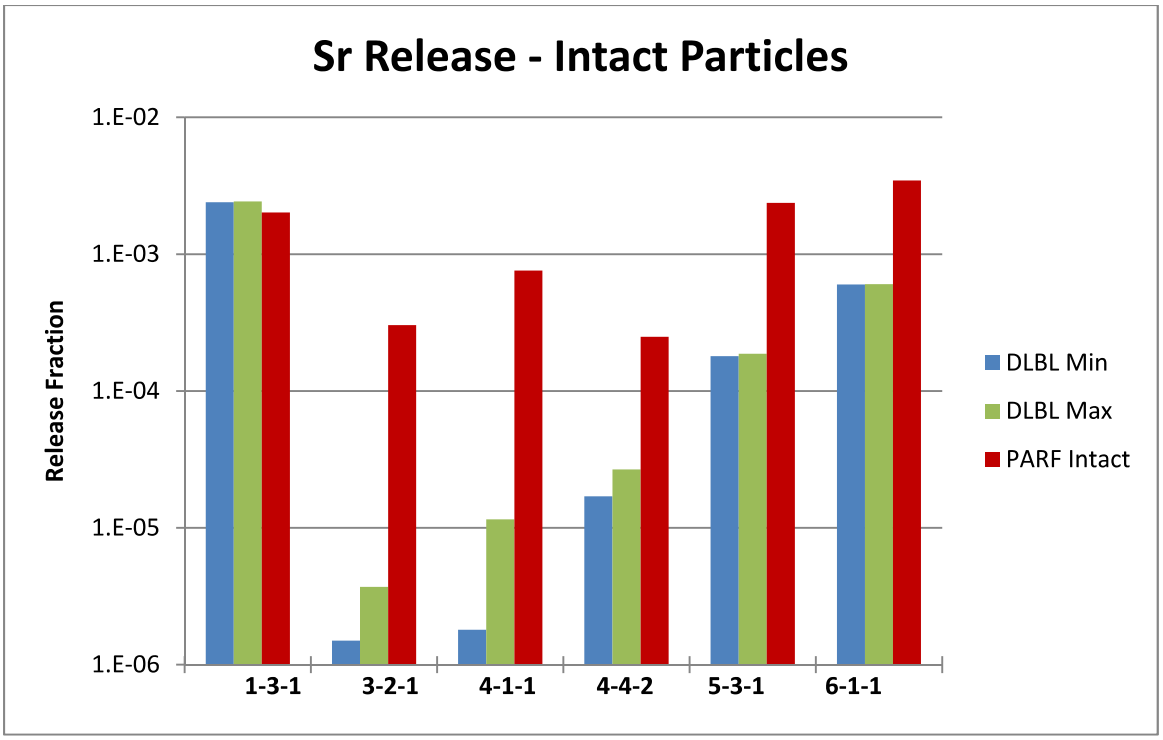

Figure 25. Strontium fractional release from compacts containing intact particles only.

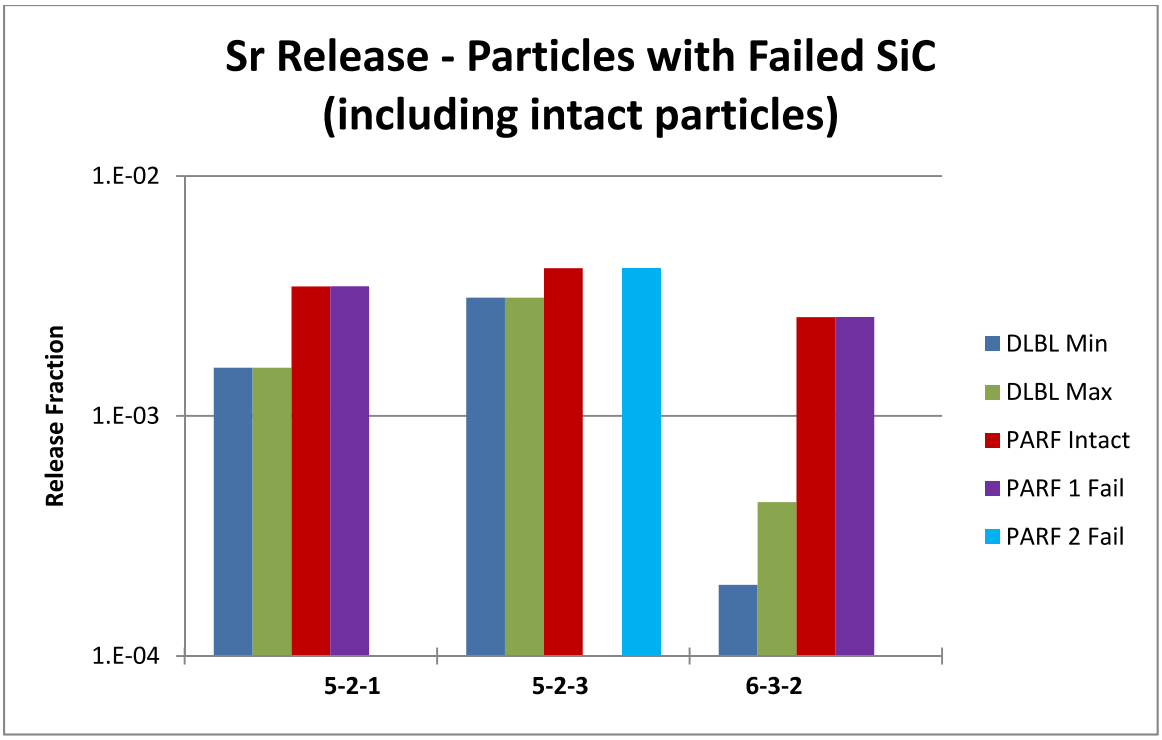

Figure 26. Strontium fractional release from compacts containing particles with failed SiC layers. PARFUME predictions include the release from intact particles.

5.2 Discussion and Analysis on Cesium and Strontium Release

Figure 23 shows that, on average, PARFUME overpredicts the measured cesium release from intact particles by up to two orders of magnitude, with the exception of Compact 4-4-2 for which the predicted release is slightly lower than the measured release. For strontium, the PARFUME overprediction is up to 2.5 orders of magnitude, except for Compact 1-3-1 where the calculated release is slightly lower than the measured release (see Figure 25).

While comparisons between PARFUME and PIE for cesium and strontium suffer from the same issues encountered with silver (e.g., the temperature and burnup distributions that are not taken into account in the modeling make it difficult to make detailed predictions), the magnitude of the discrepancy in the measured versus calculated release from intact particles is striking. PARFUME's overprediction of the release of cesium and strontium indicates that the IAEA diffusivities of these species in SiC are too high at the AGR-1 irradiation temperatures.

Figure 24 shows the contribution to the release of cesium from one or two particles with failed SiC is slightly overestimated by PARFUME. The PARFUME predictions PARF N Fail in Figure 24 exclude the contribution of intact particles, as PIE showed the release is dominated by the contribution of particles with failed SiC. A failed SiC layer gives direct access to the diffusivity in the kernel, assuming the PyC layers are lowly retentive and there is no holdup of cesium due to the formation of immobile species elsewhere within the particle. Figure 24 seems then to indicate the IAEA diffusivity of cesium in the kernel is too high. This could also explain why the predicted cesium release is too high in intact particles, as shown in Figure 23. It could therefore be expected that the diffusivity of cesium in UCO is lower than its diffusivity in UO_2, the latter being used in the PARFUME modeling due to a lack of empirical data for UCO. Based on Figure 24, the predicted fractional release is about a factor of two higher than the PIE measurements, which at this relatively high level of cesium release corresponds to an overestimation of the diffusivity of cesium in the kernel by a factor of about 100. In addition, although the cesium release

from intact particles is much lower than from particles with a failed SiC layer, the larger relative discrepancy between PARFUME calculations and PIE data on the release from intact particles would indicate that the diffusivity of cesium in SiC given by the IAEA is also too high at the AGR-1 irradiation temperatures. Taking into account the correction on the diffusivity of cesium in the kernel, the overprediction of its diffusivity in SiC would be around 30%.

As mentioned in Section 3.4, the failure of coating layers is modeled in PARFUME from the beginning of irradiation, while it is theoretically predicted that any potential failure would occur after about 100 EFPD. This leads to a shift of 100 days in cesium release. Figure 27 shows how cesium release is predicted by PARFUME for Compacts 5-2-3 and 6-3-2. It takes about 400 days for cesium to diffuse all the way through the kernel and PyC layers, according to the IAEA diffusivities used in the modeling. Shifting the curves by 100 days would not significantly impact the final cesium release. The overprediction of cesium release observed in Figure 24 can therefore hardly be explained by the timing of the SiC failures unless these failures appeared much later during irradiation, which is not an assumption supported by stress analysis.

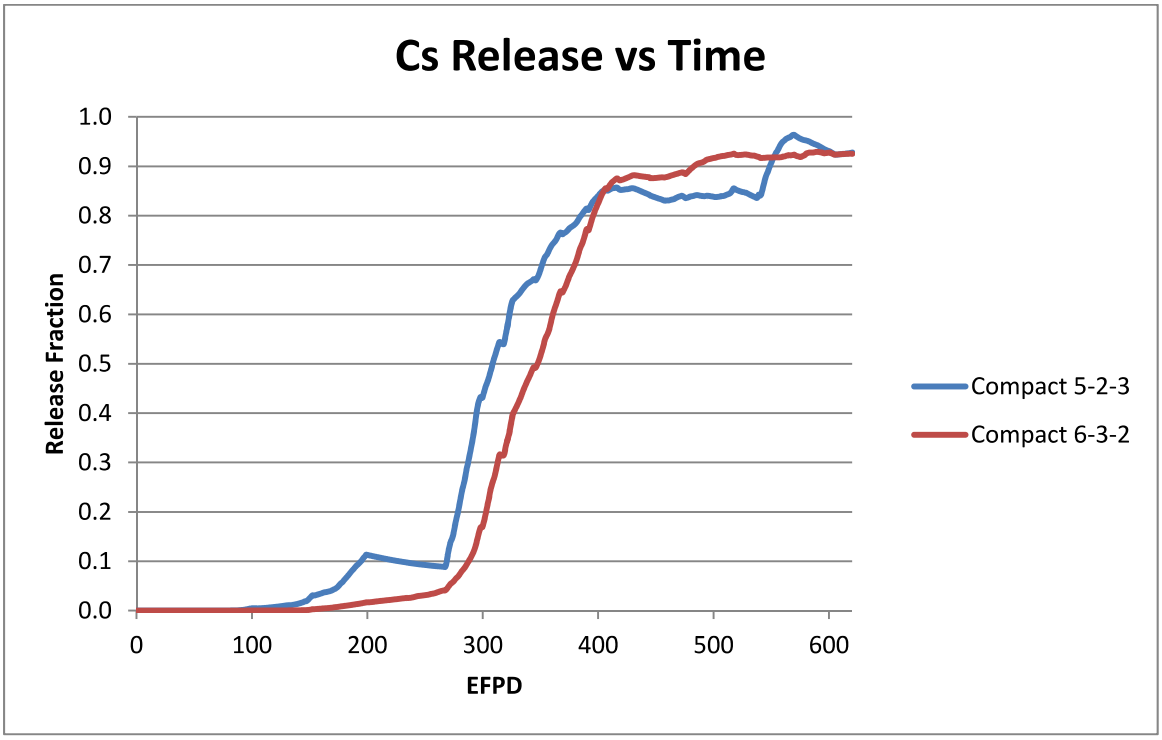

Figure 27. Cesium release over time for Compacts 5-2-3 and 6-3-2.

In the case of strontium, the available PIE data do not allow a conclusive assessment of the overprediction of the diffusivities in the kernel or SiC layer since the respective contributions from intact particles and particles with failed SiC are not clearly separable. The PARFUME predictions in Figure 26 include the contribution of intact particles, as PIE showed it was not negligible compared to the release from particles with failed SiC. Figure 25 shows a large overprediction of the release from intact particles in most cases (with the exception of Compact 1-3-1). This overprediction is also evident in Figure 26 for Compact 6-3-2, though it is much more limited for Compacts 5-2-1 and 5-2-3. Figure 26 shows the release fraction of strontium from Compact 5-2-3 is about 0.3%. The contribution to the release fraction from particles with failed SiC cannot exceed 4.8×10^{-4}, corresponding to two failed particles out of ~4,150 in the compact. Therefore, most of the measured release from Compact 5-2-3 comes from the intact particles. Similarly, the release from the intact particles of Compact 5-2-1 is approximately 0.16%, making up most of the compact release despite having one particle with failed SiC. Such a high release

from intact particles would be consistent with the release observed from Compact 1-3-1 (see Figure 25) but does not offer any indication about the strontium release from particles with failed SiC. In this case, the overprediction observed on the release from intact particles can be attributed to an overestimation of the effective diffusivity of strontium in SiC, or in UCO, or both. It would also be possible one diffusivity is overestimated while the other is under-estimated, with the larger magnitude of the overestimation leading to the overall overprediction on the release.

This basic analysis on cesium and strontium is conducted on very limited statistics including a few compacts (4-4-2 and 1-3-1, and possibly 6-3-2) that do not follow the overall trend, and with the limitation due to the simplified PARFUME modeling. As it is the case with silver, conclusions regarding cesium and strontium must therefore be embraced with care. The same overall summary derived for silver also applies to cesium and strontium (see Section 4.4.4).

6. CONCLUSION

The PARFUME modeling code was used to predict fission product release from TRISO-coated fuel particles and compacts during the AGR-1 irradiation, and compare the predictions to PIE measurements.

Comparisons between PARFUME and PIE were conducted on the release of fission products silver, cesium, and strontium, both at the particle and compact levels. Post-irradiation examination measurements were made by gamma scanning of 56 compacts, IMGA on particles from nine deconsolidated compacts for silver, by DLBL of nine compacts for cesium and strontium, and measurement of silver, cesium, and strontium on the irradiation capsule components.

The results of these comparisons are summarized below:

- Silver
  - PARFUME predictions and PIE measurements are in reasonably good agreement.
  - The large distribution in silver release from IMGA measurements can be partially explained by the spatial distribution of temperatures across a compact, as demonstrated by PARFUME calculations.
  - Low burnup capsules tend to have a higher silver release because they became hotter towards the end of irradiation when silver was readily available for release. Both PARFUME calculations and PIE data show this trend of higher release at lower burnup, but it is more strongly marked in PIE measurements.
  - PARFUME tends to under-predict PIE in the lower burnup capsules and to overpredict PIE in the higher burnup capsules.
  - PIE data suggest significant retention of silver by the matrix, though it is not predicted by PARFUME due to its historical high diffusivity of silver through graphite.
- Cesium
  - The predicted cesium release from particles with failed SiC is too high by a factor of about two, which could mean that the IAEA diffusivity of cesium in the kernel (UO_2 by default in PARFUME) is also too high. Consequently, the diffusivity of cesium in UCO could be lower than its diffusivity in UO_2 by a factor of about 100.
  - There is an overall overprediction by PARFUME of cesium release from intact particles by an order of magnitude. Taking into account the overprediction in kernel diffusivity, then the IAEA diffusivity of cesium in SiC is too high by about 30%.
- Strontium
  - The release from intact particles is large enough so that the contribution from a few particles with failed SiC cannot be assessed. Furthermore, the PIE data are too scarce to draw conclusions about the validity of the diffusivity of strontium in UCO.
  - There is an overall overprediction by PARFUME of strontium release, suggesting that the IAEA diffusivities of strontium in SiC, UCO or both are too high. The data do not allow a straightforward derivation of more suitable diffusion coefficients for strontium in UCO or SiC.

It should be duly noted that these conclusions rest upon results obtained on a relatively small number of specimens (especially for cesium and strontium) and with a modeling issue with temperature and burnup spatial distributions across the compacts. Some conclusions have a reasonable level of confidence, but the analysis in terms of correct values of the diffusivities is only tentative. As detailed in Section 4.4.4, there are major factors affecting both the data and calculations used in this fractional release assessment, namely:

- Accuracy of the diffusivities (PARFUME)
- Accuracy of the predicted compact temperatures (PARFUME)
- Spatial distribution of the compact daily temperatures (PARFUME)
- Spatial distribution of the sources (PARFUME)
- Uncertainty from gamma scanning measurements (PIE)
- Predicted Ag-110m activity in the case of silver (PIE).

Refining the modeling with spatial burnup and temperature distributions would allow better predictions of the fractional release of the fission products and more accurate comparisons between model predictions and compact gamma scanning or leach-burn-leach results. Comparison with IMGA results poses an additional problem of unknown specific irradiation conditions experienced by the subset of particles, which is related to their original location within the compacts, which does not seem to be easily solved.

7. REFERENCES

American Society of Mechanical Engineers, "NQA-1-2008; 1a-2009 Quality Assurance Requirements for Nuclear Facility Applications," March 2008 (Addenda August 2009).

CEGA Corporation, "NP-MHTGR Material Models of Pyrocarbon and Pyrolytic Silicon Carbide," CEGA-002820, Rev. 1, July 1993.

Collin, B. P., "AGR-2 Irradiation Experiment Test Plan," PLN-3798, Rev. 1, October 2011.

Collin, B. P., "AGR-1 Irradiation Test Final As-Run Report," INL/EXT-10-18097, Rev. 2, August 2014.

Croff, A.G., "ORIGEN2: A Versatile Computer Code for Calculating the Nuclide Compositions and Characteristics of Nuclear Materials, Nuclear Technology," Vol. 62, pp. 335–352, 1983.

Demkowicz, P. A., "AGR-1 Post-Irradiation Examination Plan," PLN-2828, Rev. 1, March 2010.

Demkowicz, P. A., J. D., Hunn, R. N., Morris, J. M., Harp, P. L.,, Winston, C. A., Baldwin, and F. C., Montgomery, "Preliminary Results of Post-Irradiation Examination of the AGR-1 TRISO Fuel Compacts," HTR2012-3-021, Proceedings of the HTR2012 Conference, Tokyo, Japan, October 28 --November 1, 2012.

Demkowicz, P. A., J. M., Harp, P. L., Winston, S. A., Ploger, "Analysis of Fission Products on the AGR-1 Capsule Components", INL/EXT-13-28463, March 2013.

Demkowicz, P. A., Hunn, J. D., Ploger, S. A., Morris, R. N., Baldwin, C. A., Harp, J. M., Winston, P. L., Gerczak, T. J., van Rooyen, I. J., Montgomery, F. C., Silva, C. M., "Irradiation performance of AGR-1 high temperature reactor fuel," HTR2014-31182, Proceedings of the HTR2014 Conference, Weihai, China, October 27–31, 2014.

Harp, J. M., P. A., Demkowicz, S. A., Ploger, "Post-irradiation examination and fission product inventory analysis of AGR-1 irradiation capsules," HTR2012-3-006, Proceedings the of HTR2012 Conference, Tokyo, Japan, October 28–November 1, 2012.

Harp, J. M., "Analysis of Individual Compact Fission Product Inventory and Burnup for the AGR-1 TRISO Experiment using Gamma Spectrometry," ECAR 1682, Rev. 2, June 2013.

Hawkes, G. L., "AGR-1 Daily As-run Thermal Analyses," ECAR-968, Rev. 2, January 2012.

Hunn, J. D., C. A., Baldwin, T. J., Gerczak, F. C., Montgomery, R. N., Morris, C. M., Silva, P. A., Demkowicz, J. M., Harp, S. A., Ploger, I. J., van Rooyen, K. E., Wright, "Detection and analysis of particles with breached SiC in AGR-1 fuel compacts," HTR2014-31254, Proceedings of the HTR2014 Conference, Weihai, China, October 27–31, 2014.

IAEA, "Fuel performance and fission product behaviour in gas cooled reactors," TECDOC-978, November 1997.

LANL, X-5 Monte Carlo Team, "MCNP—A General Monte Carlo N-Particle Transport Code, Version 5," Volume I, LA-UR-03-1987, Los Alamos National Laboratory, April 24, 2003 (Revised June 30, 2004) and Volume II, LA-CP-0245, Los Alamos National Laboratory, April 24, 2003 (Revised June 30, 2004).

Longhurst, G. R., D. F., Holland, J. L., Jones, B. J., Merrill, "TMAP4 User's Manual," EGG-FSP-10315, June 1992.

Maki, J. T., "AGR-1 Irradiation Experiment Test Plan," INL/EXT-05-00593, Rev. 3, October 2009.

Miller, G. K., and D. L., Knudson, "AGR-1 Pre-Test Prediction Analysis using the PARFUME Code," EDF-5741, Rev. 1, April 2007.

Miller, G. K., D. A., Petti, J. T., Maki, D. L., Knudson, "PARFUME Theory and Model Basis Report," INL/EXT-08-14497, September 2009.

Morris, R. N., P. A., Demkowicz, J. D., Hunn, C. A., Baldwin, E. L., Reber, "Performance of AGR-1 high temperature reactor fuel during post-irradiation heating tests," HTR2014-31135, Proceedings of the HTR2014 Conference, Weihai, China, October 27–31, 2014.

Simonds, J., "Technical Program Plan for the Very High Temperature Reactor Technology Development Office/Advanced Gas Reactor Fuel Development and Qualification Program," PLN-3636, Rev. 3, May 2014.

Sterbentz, J. W., "JMOCUP As-Run Daily Depletion Calculation for the AGR-1 Experiment in ATR B-10 position," ECAR-958, Rev. 1, August 2011.

Sterbentz, J. W., "JMOCUP As-Run Daily Depletion Calculation for the AGR-1 Experiment in ATR B-10 position," ECAR-958, Rev. 2, September 2013.

Appendix A

COMPACT DISTRIBUTION FOR BURNUP, FAST FLUENCE, AND TEMPERATURE

APPENDIX A
Compact Distribution For Burnup, Fast Fluence, And Temperature

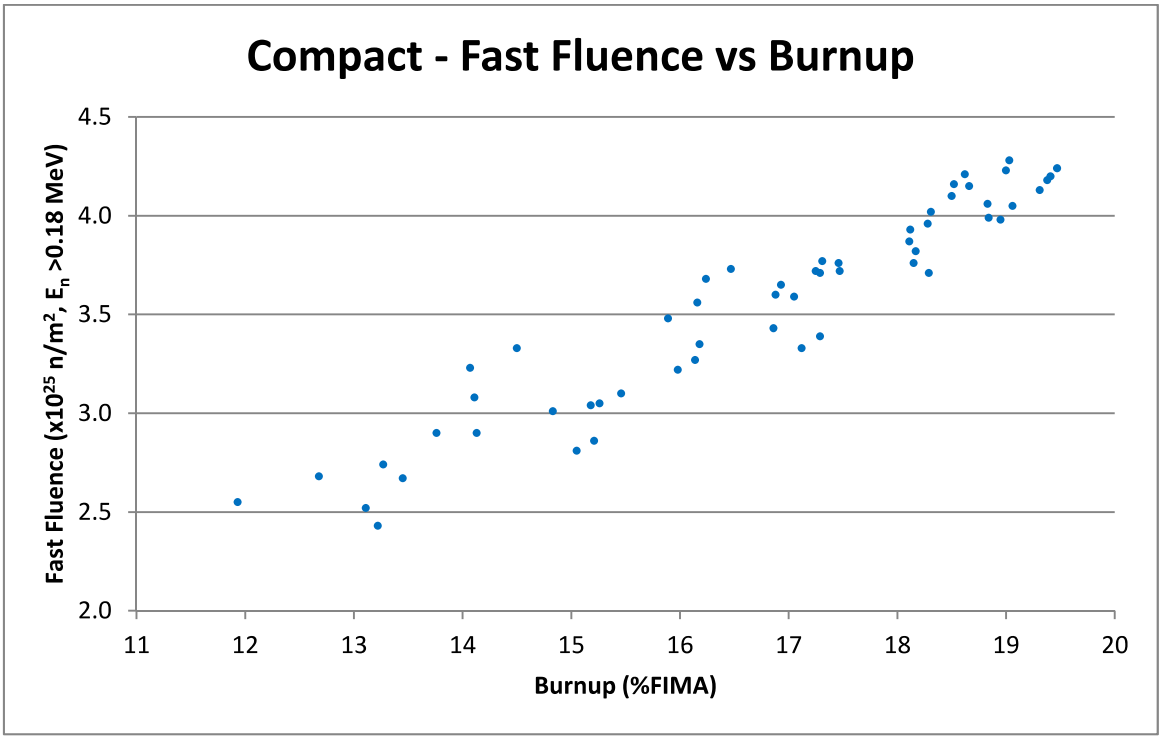

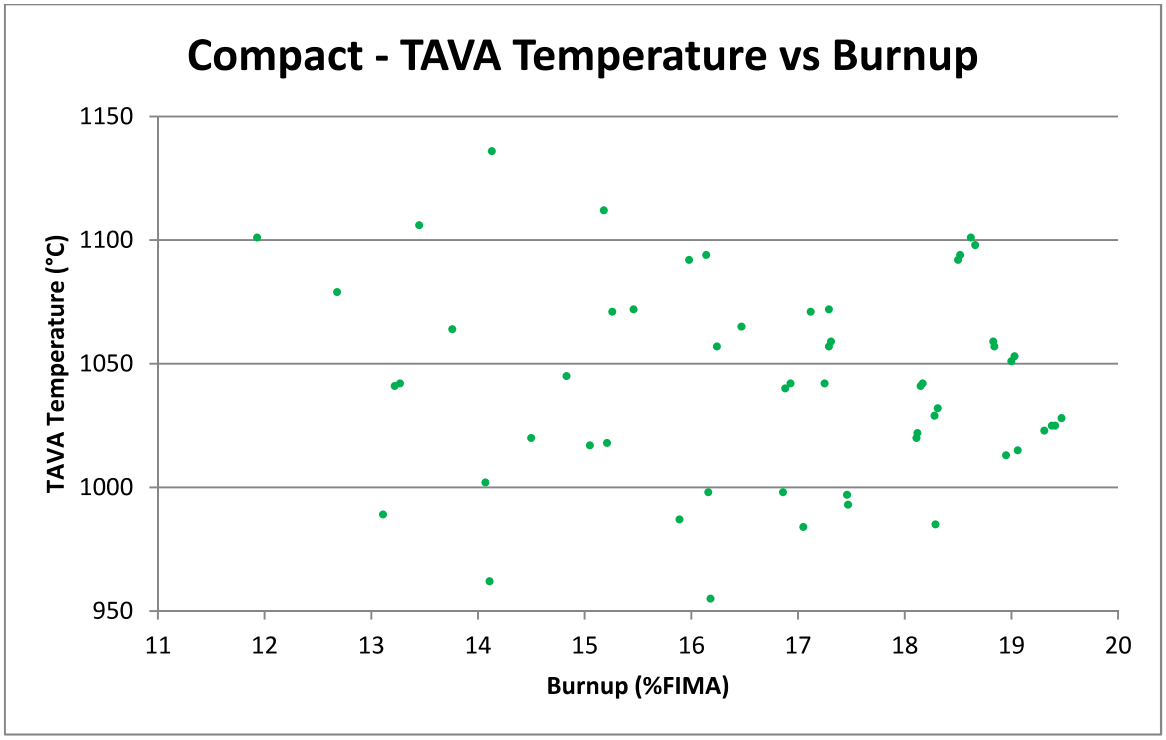

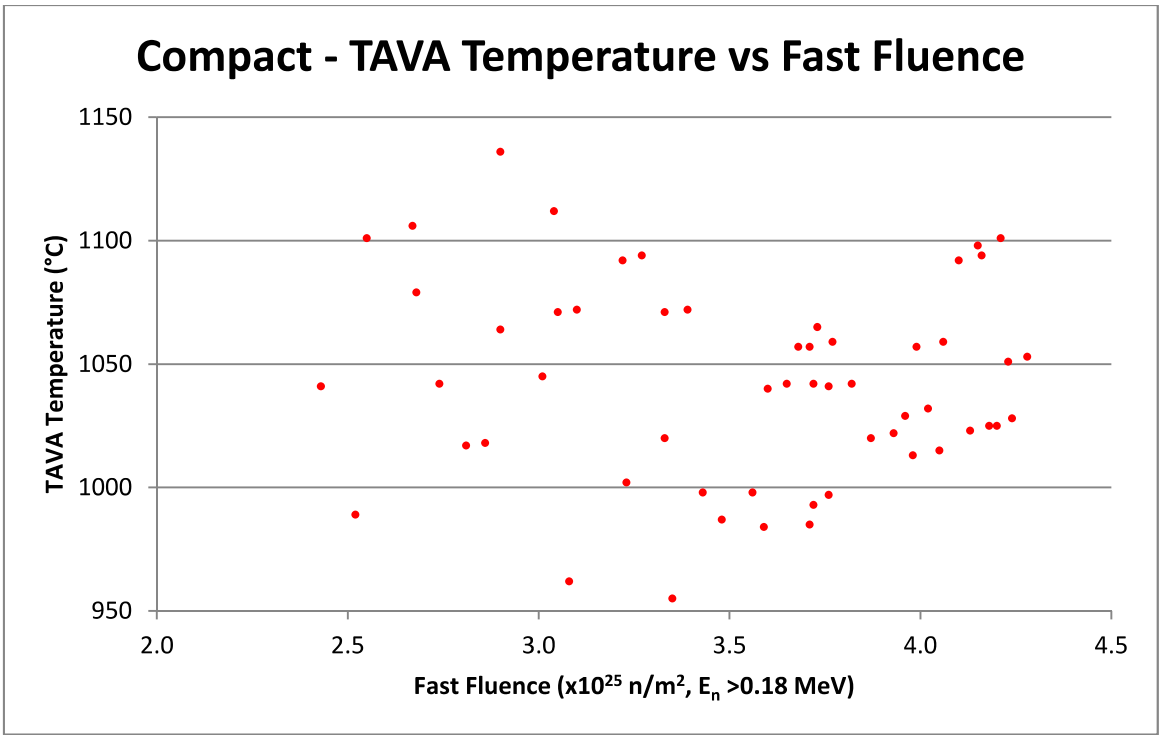
Compact - TAVA Temperature vs Fast Fluence
TAVA Temperature (°C)
1150
1100
1050
1000
950
2.0
2.5
3.0
3.5
4.0
4.5
Fast Fluence (x10^25 n/m^2, E_n >0.18 MeV)

Appendix B

AG RELEASE FROM COMPACT GAMMA SCANNING PER CAPSULE

APPENDIX B
Ag Release From Compact Gamma Scanning Per Capsule

See Table 1 in Section 2 for compact numbering.

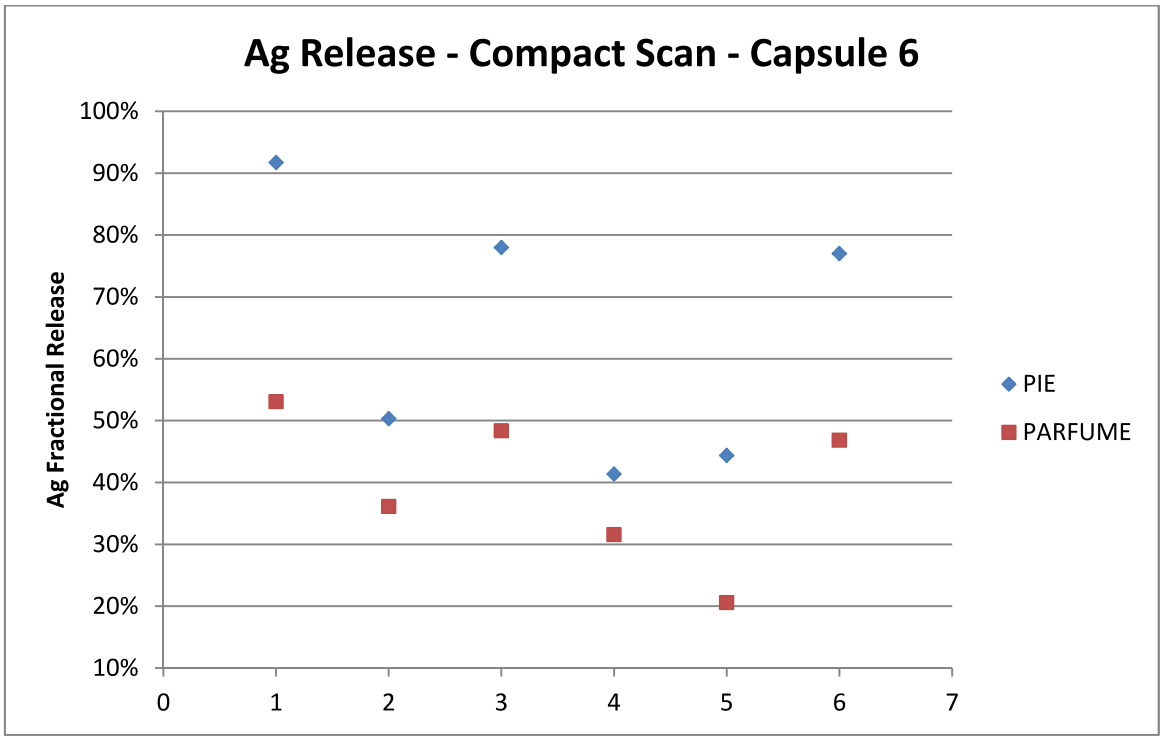

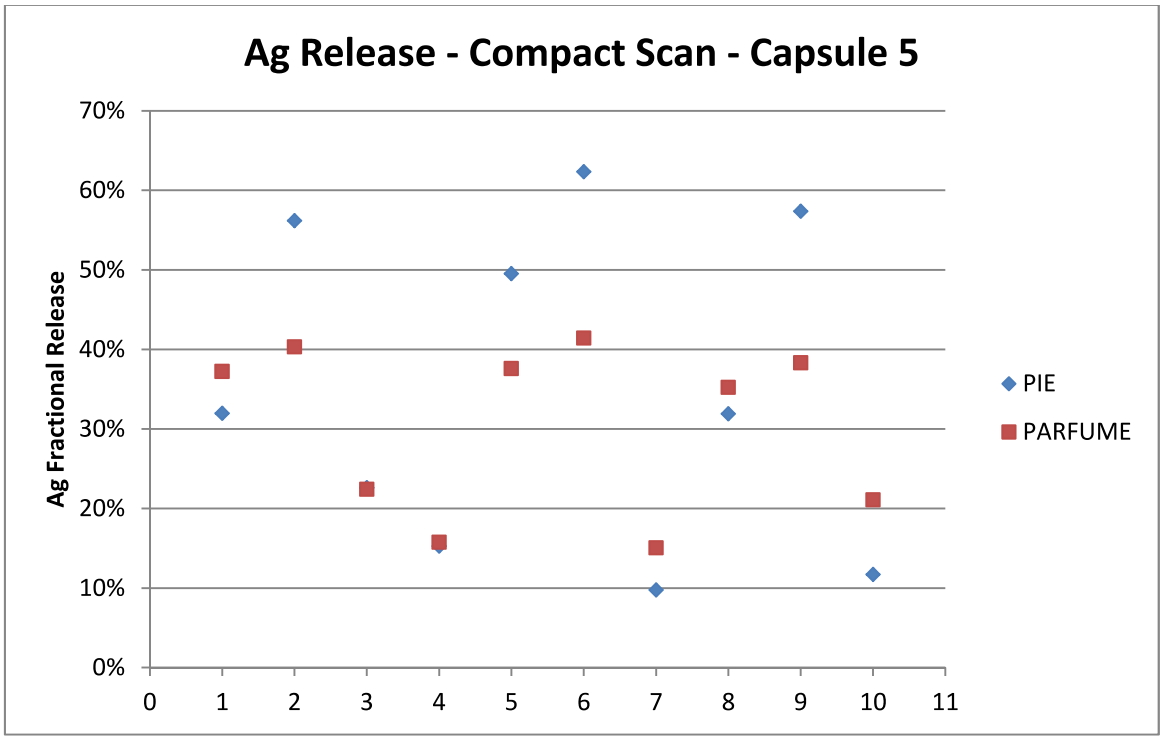

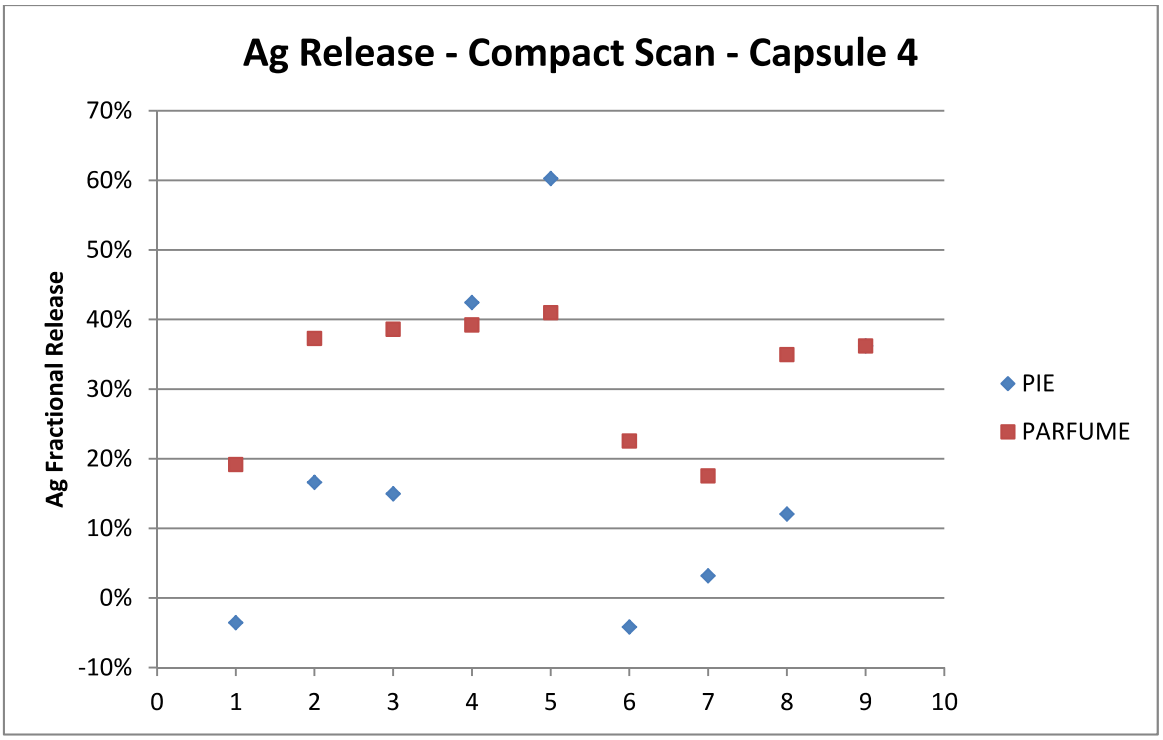
Ag Release - Compact Scan - Capsule 4
Ag Fractional Release
70%
60%
50%
40%
30%
20%
10%
0%
-10%
0
1
2
3
4
5
6
7
8
9
10
PIE
PARFUME

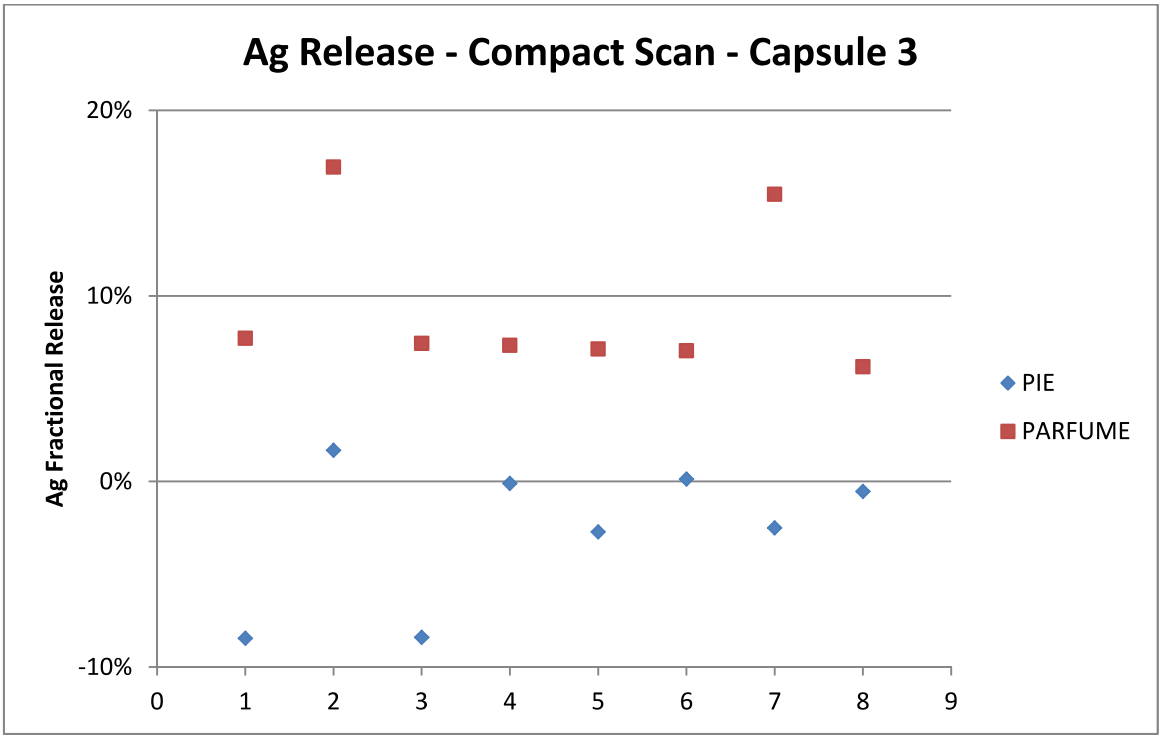
Ag Release - Compact Scan - Capsule 3
Ag Fractional Release
20%
10%
0%
-10%
0
1
2
3
4
5
6
7
8
9
PIE
PARFUME

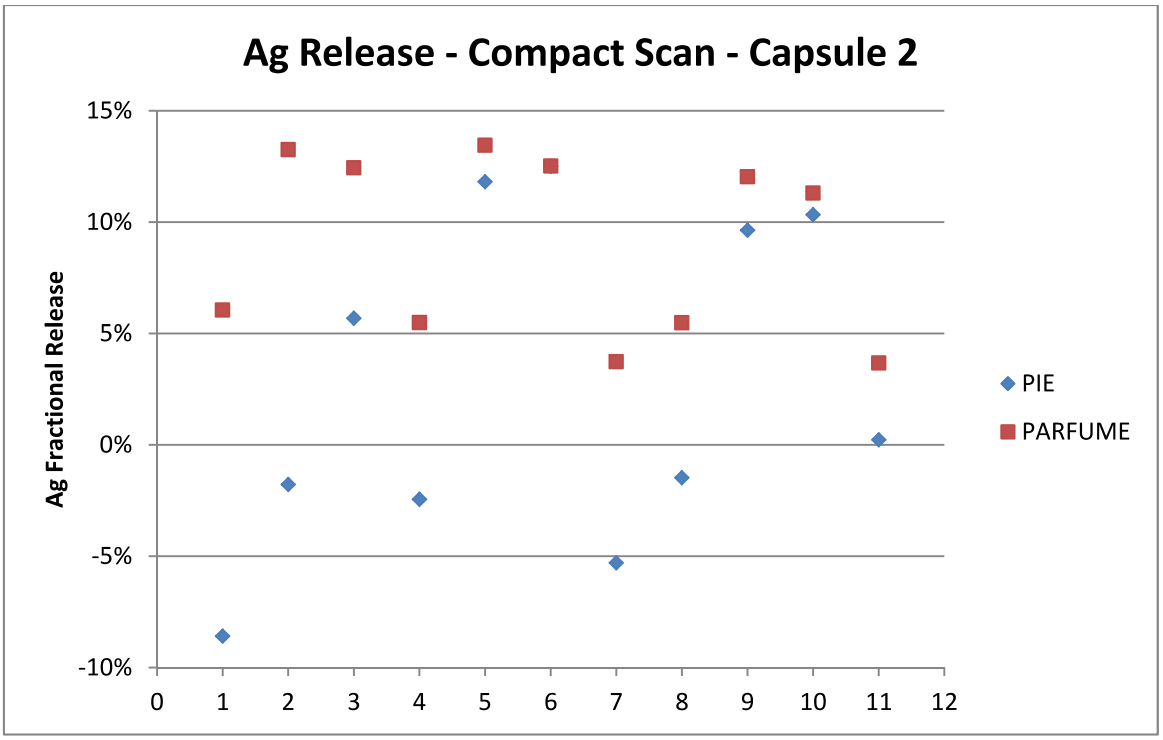
Ag Release - Compact Scan - Capsule 2
Ag Fractional Release
15%
10%
5%
0%
-5%
-10%
0
1
2
3
4
5
6
7
8
9
10
11
12
PIE
PARFUME

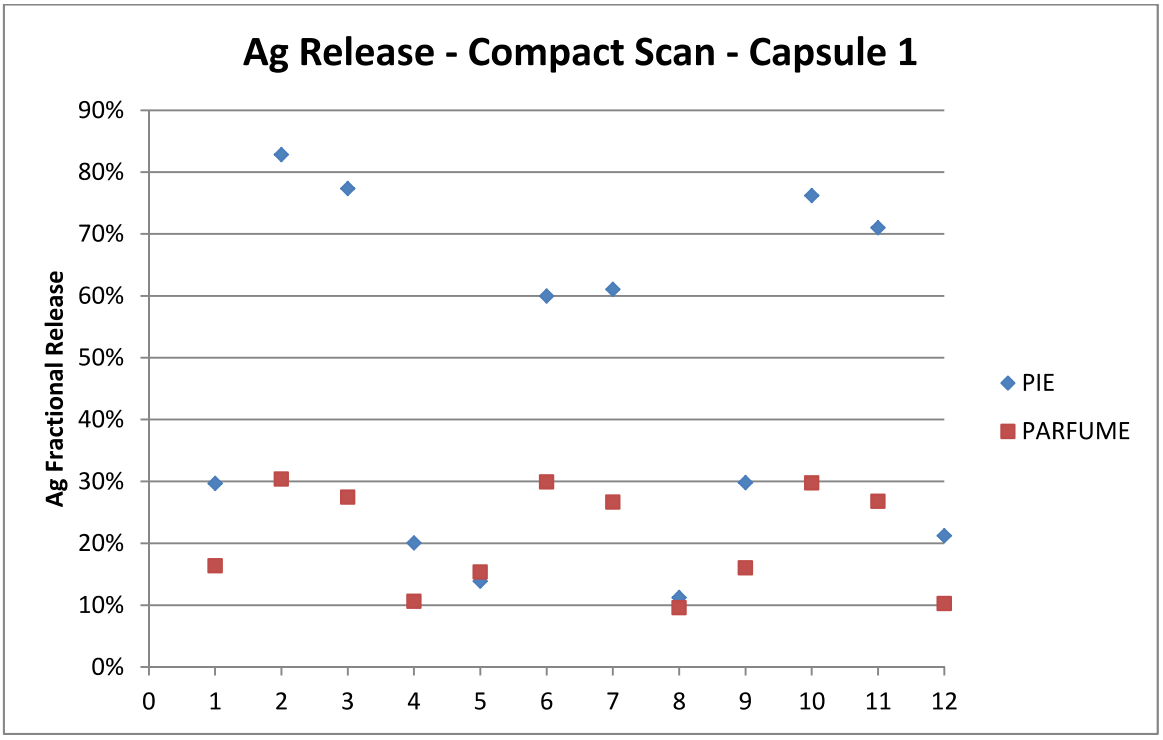
Ag Release - Compact Scan - Capsule 1
Ag Fractional Release
90%
80%
70%
60%
50%
40%
30%
20%
10%
0%
0
1
2
3
4
5
6
7
8
9
10
11
12
PIE
PARFUME

Appendix C

AG RELEASE FROM COMPACT VERSUS BURNUP, FAST FLUENCE, AND TEMPERATURE

APPENDIX C
Ag Release From Compact Versus Burnup, Fast Fluence, And Temperature

See Table 1 in Section 2 for compact numbering.

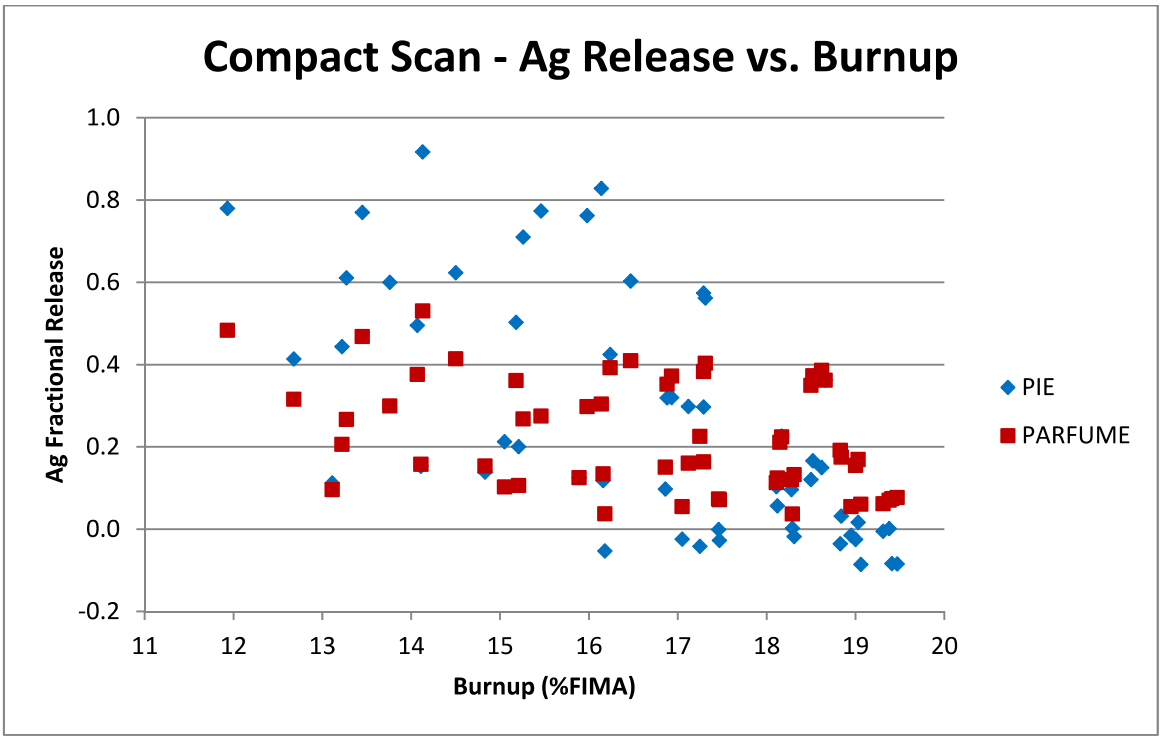

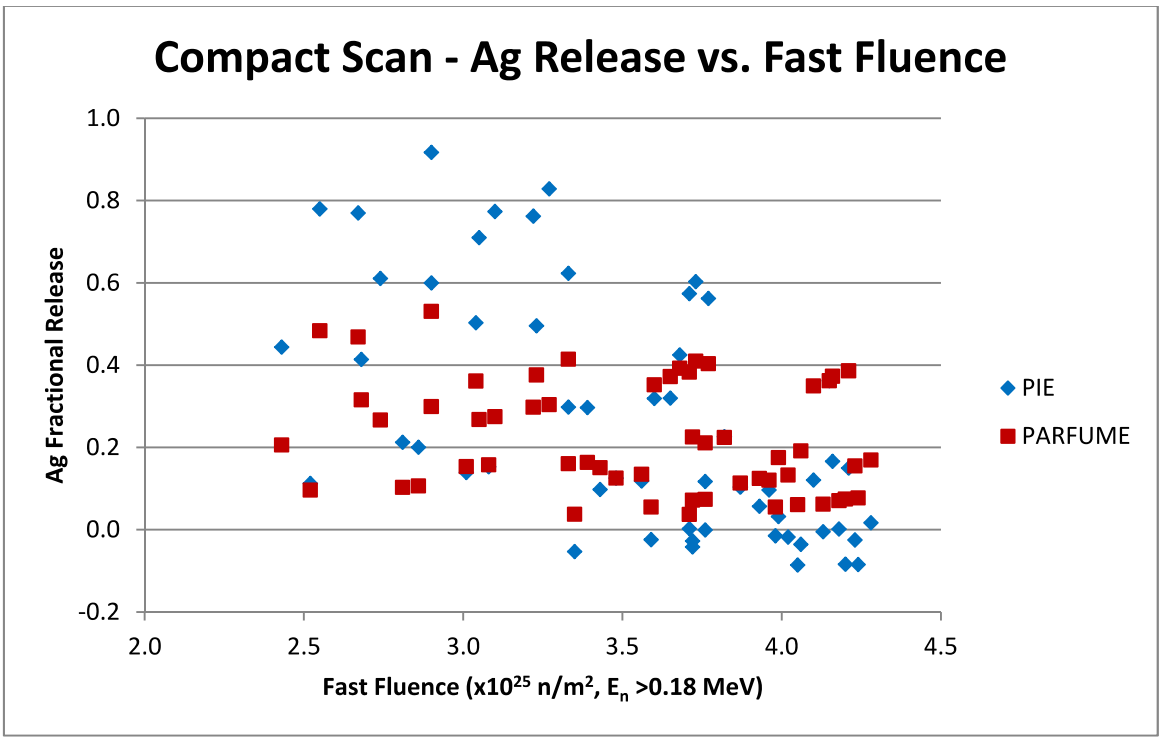

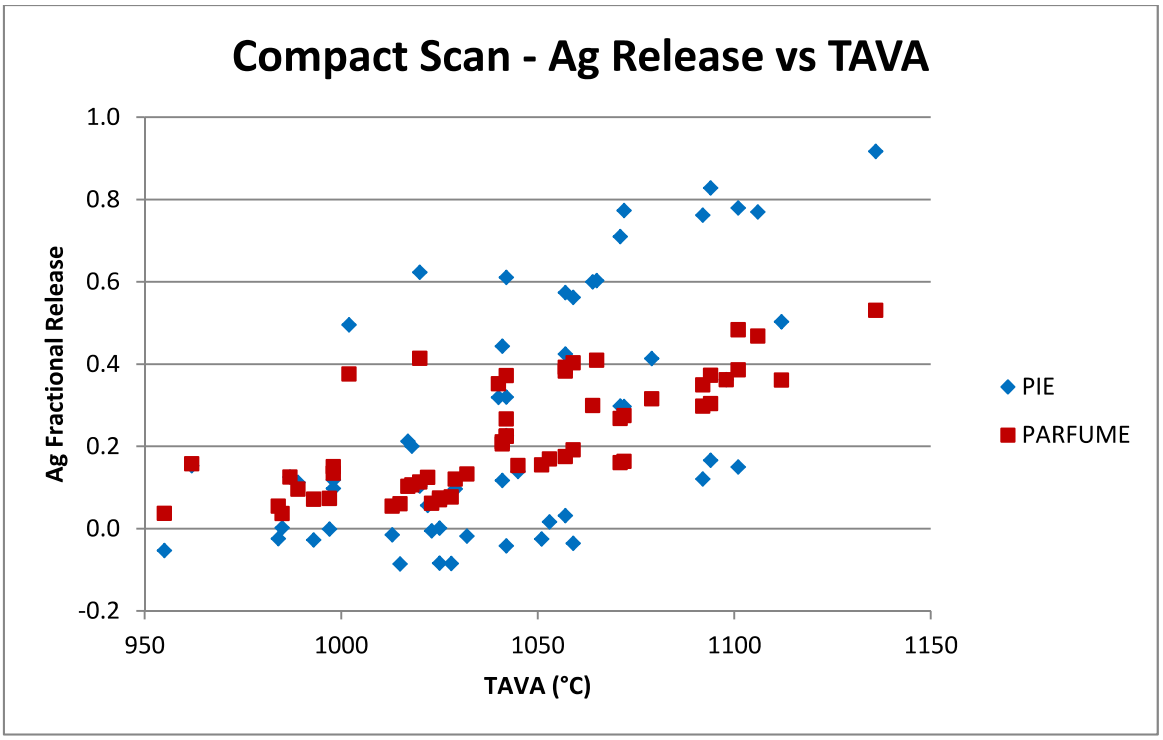
Compact Scan - Ag Release vs TAVA
Ag Fractional Release
1.0
0.8
0.6
0.4
0.2
0.0
-0.2
950
1000
1050
1100
1150
TAVA (°C)
PIE
PARFUME

Appendix D

CONSIDERATIONS ON RELEASE COMPARISON

APPENDIX D
Considerations On Release Comparison

This appendix presents theoretical considerations on the comparison between the release fractions calculated by PARFUME, and assessed by PIE using a fission product source obtained from as-run neutronics calculations.

The theoretical development considers a compact with N particles. For each particle "i", the fission product release R_i is given by the relation:

$$R_i = f(T_i) * S(BU_i)$$

where:

T_i temperature of the particle

BU_i burnup of the particle

f release fraction of the particle (temperature dependent)

S fission product source of the particle (burnup dependent)

For the sake of simplicity, it is assumed that each particle experiences a steady temperature throughout irradiation. Since diffusion is modeled by a temperature-dependent law, the release fraction is assumed to only depend on temperature. It does not depend on the magnitude of the source, as multiplying the source by a given factor generates a release that is multiplied by the same factor, hence leaving the release fraction unchanged.

At the compact level, the total release is given by:

$$R_C = \sum_{i=1}^{N} R_i$$

and the fission product source associated with the compact is:

$$S_C = \sum_{i=1}^{N} S(BU_i)$$

This release and source reflect the real state of the compact, as experienced during irradiation.

Using the average compact burnup BU_0 and average temperature T_0, it is possible to define the release R_0 of an average particle:

$$R_0 = f(T_0) * S(BU_0)$$

where:

$$T_0 = \frac{1}{N}\sum_{i=1}^{N} T_i$$

$$BU_0 = \frac{1}{N}\sum_{i=1}^{N} BU_i$$

and the source associated with the average particle is:

$$S_0 = S(BU_0) = S\left(\frac{1}{N}\sum_{i=1}^{N} BU_i\right)$$

In PARFUME, the modeling is made on the average particle, with a source S_0 and a release R_0. In PIE, the release is measured and it is normalized to the calculated compact average source given by as-run neutronics calculations as:

$$S_C^{as-run} = N * S_0$$

PARFUME and as-run neutronics calculations have the same source S_0 assuming they use the same fission rate and fission product yield. Any difference in these values would lead to a different fission product source.

In general, this "as-run" source differs from the real source as:

$$N * S\left(\frac{1}{N}\sum_{i=1}^{N} BU_i\right) \neq \sum_{i=1}^{N} S(BU_i)$$

The equality is obtained only if the source of individual particles is linear with burnup.

As far as the comparison between PARFUME and PIE is concerned, the respective release fractions for the compact are:

$$F_C^{PIE} = \frac{R_C}{S_C^{as-run}} = \frac{\sum_{i=1}^{N} R_i}{N * S_0} = \frac{1}{N * S_0} * \sum_{i=1}^{N}\left(f(T_i) * S(BU_i)\right)$$

$$F_C^{PARF} = \frac{R_0}{S_0} = \frac{f(T_0) * S(BU_0)}{S_0} = \frac{1}{S_0} * f\left(\frac{1}{N}\sum_{i=1}^{N} T_i\right) * S\left(\frac{1}{N}\sum_{i=1}^{N} BU_i\right)$$

while the real release fraction is given by:

$$F_C = \frac{R_C}{S_C} = \frac{\sum_{i=1}^{N} R_i}{\sum_{i=1}^{N} S(BU_i)} = \sum_{i=1}^{N}\left(f(T_i) * S(BU_i)\right) \Big/ \sum_{i=1}^{N} S(BU_i)$$

These two first quantities are different unless both following conditions are verified:

- The temperature is uniform across the compact: $T_i = T_{uni}$
- The source is linear with burnup: $S(BU_i) = \alpha * BU_i$

The first condition allows writing:

$$F_C^{PIE} = \frac{f(T_{uni})}{N * S_0} * \sum_{i=1}^{N} S(BU_i)$$

and

$$F_C^{PARF} = \frac{f(T_{uni})}{S_0} * S\left(\frac{1}{N}\sum_{i=1}^{N} BU_i\right)$$

while the second condition implies:

$$F_C^{PIE} = \frac{f(T_{uni})}{N * S_0} * \sum_{i=1}^{N} (\alpha * BU_i)$$

and

$$F_C^{PARF} = \frac{f(T_{uni})}{S_0} * \alpha * \frac{1}{N} \sum_{i=1}^{N} BU_i$$

which results in identical release fractions.

If a subset of M particles is considered, the release of the subset is:

$$F_S = \sum_{j=1}^{M} R_j$$

and the associated source is:

$$S_S = \sum_{j=1}^{M} S(BU_j)$$

The normalization of the PIE measurements is made using the following source:

$$S_C^{as-run} = M * S_0$$

which again is different from the real source.

The release fraction of the subset of particles is:

$$F_S^{PIE} = \frac{1}{M * S_0} * \sum_{j=1}^{M} \left(f(T_j) * S(BU_j) \right)$$

In this case, it is equal to the calculated PARFUME release only if:

- The temperature is uniform across the compact: $T_j = T_{uni}$
- The burnup is uniform across the compact: $BU_j = BU_{uni}$

The first condition allows writing:

$$F_S^{PIE} = \frac{f(T_{uni})}{M * S_0} * \sum_{j=1}^{M} S(BU_j)$$

To equal this release fraction to the PARFUME-calculated release fraction, the linearity of the source with burnup is not sufficient anymore as the average source burnup of the subset of particles is not equal to the average burnup of the compact. Therefore, a stronger hypothesis has to be made, which is the uniformity of the burnup across the compact. In this case:

$$F_S^{PIE} = \frac{f(T_{uni})}{M * S_0} * M * S(BU_{uni})$$

and

$$F_C^{PARF} = \frac{f(T_{uni})}{S_0} * S(BU_{uni})$$

which results in identical release fractions.

Burnup dependence of the source

The plot below shows the typical fission product production of silver, cesium, and strontium during irradiation.

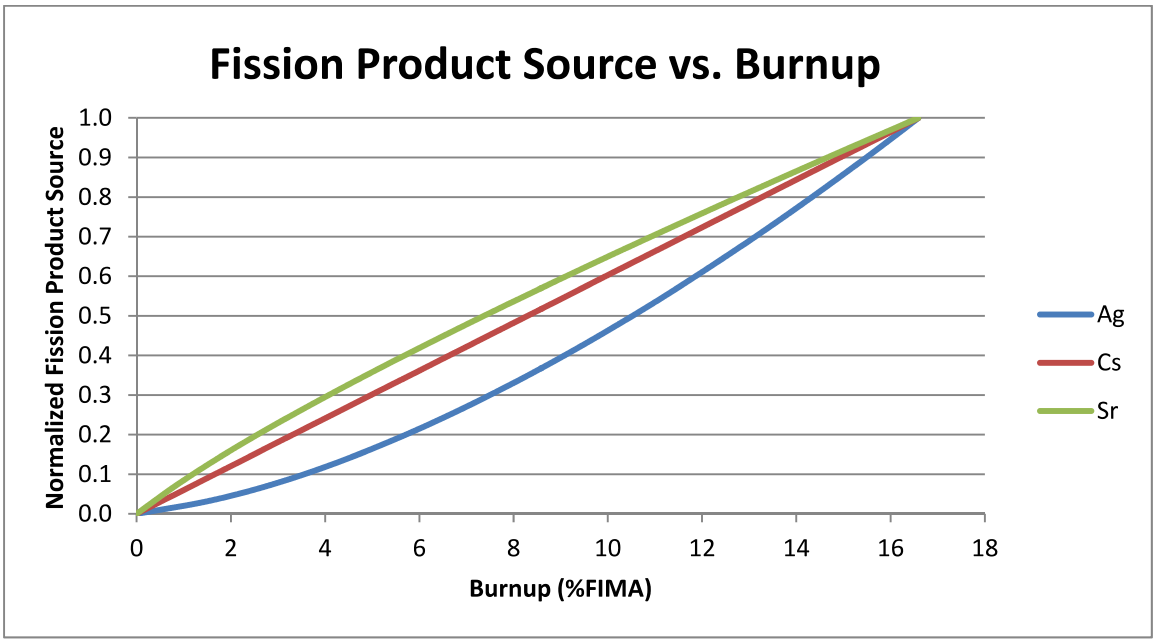

The fission yields of Ag and Sr have a dependence on burnup, while the fission yield of Cs does not have any. For the three fission product species, the resulting source can be written as:

$$S(BU) = \alpha * (BU)^n$$

With:

- Ag: $n \approx 1.5$
- Cs: $n = 1$
- Sr: $n \approx 0.8$

Assuming a uniform temperature across the compact, the PIE and PARFUME release fractions are:

$$F_C^{PIE} = \frac{f(T_{uni})}{N * S_0} * \sum_{i=1}^{N} S(BU_i)$$

and

$$F_C^{PARF} = \frac{f(T_{uni})}{S_0} * S\left(\frac{1}{N}\sum_{i=1}^{N} BU_i\right)$$

which can be rewritten:

$$F_C^{PIE} = \frac{\alpha * f(T_{uni})}{S_0} * \frac{1}{N}\sum_{i=1}^{N} (BU_i)^n$$

and

$$F_C^{PARF} = \frac{\alpha * f(T_{uni})}{S_0} * \left(\frac{1}{N}\sum_{i=1}^{N} BU_i\right)^n$$

With the typical burnup values of the AGR-1 irradiation and the values of the exponents for the three fission product species, we obtain the following:

- Ag: $F_C^{PIE} < F_C^{PARF}$
- Cs: $F_C^{PIE} = F_C^{PARF}$
- Sr: $F_C^{PIE} > F_C^{PARF}$